Chapter 12

Adiabatic Concentration and Coherent Control in Nanoplasmonic Waveguides

Mark I. Stockman

Department of Physics and Astronomy, Georgia State University
Atlanta, Georgia 30303, USA

We describe ideas and results of controlling surface plasmon polaritons (SPPs) in nanoplasmonic waveguides. The adiabatic concentration of the optical energy in tapered nanoplasmonic waveguides is presented as a universal approach to transfer of energy and coherence from macro- or microscale to the nanoscale. Coherent control allows for directed and dynamically-defined concentration of the optical energy on nanometer-femtosecond spatio-temporal scale.

1. Introduction

Nanooptics and nanoplasmonics are experiencing presently a period of explosive growth and attracting a great interest. Nanoplasmonics deals with electronic processes at the surfaces of metal nanostructures, which are due to electronic excitations called surface plasmons (SPs) that can localize optical energy on the nanoscale.[1–3] The nanoplasmonic processes can potentially be the fastest in optics: their shortest evolution times are defined by the inverse spectral width of the region of the plasmonic resonances and are on the order of 100 as.[4] The relaxation times of the SP excitations are also ultrashort, in the $10 - 100$ fs range.[5–9] Such nanolocalization and ultrafast kinetics make plasmonic nanostructures promising for various applications, especially for the ultrafast computations, data control and storage on the nanoscale.

These and potentially many other applications require precise control over the optical excitations of the nanostructures in time and space on the femtosecond-nanometer scale. Such a control cannot be imposed by far-field focusing of the optical radiation because the diffraction limits its dimension to greater than half wavelength. In other words, the optical radiation does not have spatial degrees of freedom on the nanoscale. There is a different class of approaches to control a system on nanoscale based on plasmonic nanoparticles or waveguides brought to the *near-field* region of the system. Among these we mention: the tips of scanning near-field optical microscopes,[1] adiabatic plasmonic waveguides,[10] nanowires,[11,12] plasmonic superlenses[13] or hyperlenses.[14] In all these cases, massive amount of

metal is brought to the vicinity of the plasmonic nanosystem, which will produce strong perturbations of its spectrum and SP eigenmodes, cause additional optical losses, and adversely affect the ultrafast dynamics and energy nanolocalization in the system. This nanowaveguide approach also may not work because of the excitation delocalization due to the strong interaction (capacitive coupling) at the nanoscale distances for optical frequencies.

We have proposed[15] a principally different approach to ultrafast optical control on the nanoscale based on the general idea of coherent control. The coherent control of the quantum state of atom and molecules is based on the directed interference of the different quantum pathways of the optical excitation,[16–25] which is carried out by properly defining the phases of the corresponding excitation waves. This coherent control can also be imposed by an appropriate phase modulation of the excitation ultrashort (femtosecond) pulse.[22,26–28] Shaping the polarization of a femtosecond pulse has proven to be a useful tool in controlling quantum systems.[29]

Our initial idea[15] has been subsequently developed theoretically[29–32] and confirmed experimentally.[33–35] In this coherent control approach, one sends from the far-field zone a shaped pulse (generally, modulated by phase, amplitude, and polarization) that excites a wide-band packet of SP excitations in the entire nanosystem. The phases, amplitudes, and polarizations of these modes are forced by this shaped excitation pulse in such a manner that at the required moment of time and at the targeted nanosite, these modes' oscillations add in phase while at the other sites and different moments of time they interfere destructively, which brings about the desired spatio-temporal localization. Theoretically, the number of the effective degrees of freedom that a shaped femtosecond pulse may apply to a nanoplasmonic system is on the order of its quality factor Q (i.e., the number of coherent plasmonic oscillations that system undergoes before dephasing). In the optical region for noble metals $Q \sim 100$, providing a rich, ~ 100-dimensional space of controlling parameters. The coherent control approach is non-invasive: in principle, it does not perturb or change the nanosystem's material structure in any way.

The coherent control approach can be employed to control not only nanosystems, which support localized SP modes, but also extended nanostructured systems that carry surface plasmon polaritons. In this case, the phase and polarization modulation of the excitation radiation can determine the propagation pathway in a nanoplasmonic waveguide splitters.[32,36]

Even more promising is the recent idea of the full coherent control on the nanoscale.[37] The idea of this approach is a nanoplasmonic counterpart of the Active Phased Array radar (APAR), also called Active Electronically Steered Array (AESA) radar. It also incorporates ideas of the adiabatic concentration of the optical energy on nanoscale (see Sec. 2) and of time-reversal (back-tracing).

The full coherent control on the nanoscale is achieved by placing an array (possibly, a linear array) of nanoparticles on a SPP nanoplasmonic waveguide. Each such particle may be, in particular, a nanosphere, nanoshell, nano-indentation of

the surface, or simply a fragment of the surface roughness. These nanoparticles are positioned far away from each other so they can independently be excited, each by its own shaped (phase-, amplitude-, and polarization-modulated) ultrashort excitation pulse. As a result, there will be a packet of SPPs propagating from each of the nanoparticles in a non-directed way. However, as a result of the interference of these SPP waves, a propagating wavefront will be established. By a proper phase modulation, one can force all these SPP waves at every frequency to interfere coherently at a certain point of the nanoplasmonic waveguides at a defined time, creating un ultrashort and nanolocalized spike of the optical fields, i.e., fully controlled spatio-temporal localization.[37] The required phase modulation of the each of the controlling pulses can be found using the principle of back-propagation (or, time-reversal). Such a system can be called NAPAR (Nanoplasmonic Active Phased Array "Radar"). We will describe this approach in Sec. 3.

2. Adiabatic Concentration of Optical Energy on Nanoscale

2.1. *Introduction to Adiabatic Concentration in Nanoplasmonics*

A central problem of nanooptics is the commonly known impossibility to concentrate (focus) optical radiation on the nanoscale because the wavelength of light is on the microscale, many orders of magnitude too large. This problem appear to be fundamental because the electric and magnetic component of the electromagnetic field exchange energy on distances of half wave length, which is on order of a micron for optical frequencies, i.e., three orders of magnitude larger than the desired nanoscale. However, this limitation is removed in nanoplasmonics, because SPs are electrostatic excitations where the electric field and electron kinetic energy are exchanged in the process of optical oscillations.

Nevertheless, any attempts to couple a laser source to the nanoscale through, e.g., tapered fibers (see, e.g., Refs. 38–41) or by focusing on metal tips[42,43] lead to a tremendously low energy efficiency: only a very small part of the excitation energy is transferred to the nanoscale. This is due to the fact that the absorptions, scattering, and other effective cross sections of such nanosystems are still much less than the minimum size of the focal spot, which is on the microscale.

In this Section, we show that such impossibility is not a law of nature: we introduce a way to focus and concentrate the optical radiation on the nanoscale, in principle, without major losses by *exciting the propagating surface plasmon polaritons (SPPs) and then adiabatically, but as rapidly as possible, transforming them into localized surface plasmons (SPs)*. The latter are purely electric oscillations (without significant magnetic component) that can and do nano-localize.[3]

This possibility of the adiabatic transformation of the propagating SPPs, which are electromagnetic waves, into standing, non-propagating SPs has been introduced in Refs. 10,44. These publications considered various graded systems for the SPP adiabatic concentration of optical energy: a SPP waveguide consisting of a semi-

infinite metal covered by a semi-infinite dielectric with graded dielectric permittivity, a dielectric nanolayer on massive metal, and a tapered plasmonic waveguide. These systems are discussed in detail below in this Section along with the adiabatic concentration of SPPs in metal nanolayers surrounded by dielectrics and dielectric nanolayers surrounded by metal. We note that efficient adiabatic nanofocusing of SPPs has been shown theoretically also in SPP waveguides that made of nanogrooves on metal.[45] Such metal grooves have been shown experimentally to be effcient SPP waveguides.[46]

Specifically, the adiabatic transformation from the far to near zone can be done in the following way. Light waves can be transformed with high efficiency into SPPs using, e.g., a grating coupler or the well-known Kretschmann geometry. These SPPs propagate along a graded nanoplasmonic waveguide along which parameters slowly (adiabatically) change in such a way that the phase velocity of the SPPs tends to zero in the vicinity of some point at a finite distance. It is required that the excited SPP mode exists without a cut-off in the entire range of these parameters including this stopping point. Then the adiabatic theorem predicts that the wave will propagate without back-reflection and scattering into three dimensions (3D) to the stopping point. Thus this wave will adiabatically slow down and asymptotically stop at this point. This will result into the adiabatic conversion of the propagating SPPs into the stopped, quasielectrostatic SPs. At this stopping point the wavelength of the SPPs asymptotically tends to zero. This is in sharp contrast to massive (quasi)particles whose wavelength becomes infinite at the stopping point, which violates the adiabatic approximation. Note that the adiabatic approximation is called the Wentzel-Kramers-Brillouin or quasiclassical approximation in quantum mechanics.[47]

As a result of the above-described process, it is possible to adiabatically convert with high efficiency the propagating SPPs into the standing waves, which are SPs localized on the nanoscale. Being adiabatic to avoid back-reflection and scattering, this conversion nevertheless should be as rapid as possible to prevent the absorption losses in the metal. The efficiency of transformation along with maximum value of the achieved local optical fields are determined by the length of the adiabatic waveguide and the possible minimum value of the adiabatic parameter, and are limited only by the dielectric losses in the graded polaritonic waveguide.

We will consider below some examples of such systems and processes. A a metal half-space covered with semiconductor with dielectric permittivity increasing in the direction of the SPP propagation is considered in Sec. 2.2. Thin metal wedge covered with dielectric where SPPs propagate toward the sharp edge is subject of Sec. 2.6. The most energy-efficient of the graded systems considered below is a thin metal cone embedded in a dielectric, which is a subject of Sec. 2.7.

2.2. *Adiabatic Stopping of SPPs at Interface of Metal with Graded Semiconductor*

Consider a semi-infinite metal occupying a half-space of $z < 0$, whose dielectric function $\varepsilon_m(\omega)$ is uniform in space, where ω is the optical excitation frequency. The upper half-space is occupied by a dielectric or undoped semiconductor whose permittivity $\varepsilon_1(\mathbf{r})$ smoothly depends on the coordinates $\mathbf{r} = (x, y)$ in the plane (xy) of the interface. Such spatial dependence is achieved, e.g., in the well-developed semiconductor heterostructures. Using this smoothness, we will employ the eikonal approximation,[48] also called Wentzel-Kramers-Brillouin (WKB) or quasiclassical approximation[49]).

We consider SPPs as transversally-magnetic (TM) waves. For such waves, the magnetic field H_x at a plane interface between uniform metal and dielectric is given by

$$H_x(y, z, t) = H_x^{(0)} \exp\left(iky - \kappa|z| - i\omega t\right) \ , \tag{1}$$

$$E_{y,z}(y, z, t) = E_{y,z}^{(0)} \exp\left(iky - \kappa|z| - i\omega t\right) , \tag{2}$$

where $H_x^{(0)}$ and $E_{y,z}^{(0)}$ are constant amplitudes of the corresponding field components; k is the wave vector that is directed along the y axes, and κ is the corresponding evanescent exponent. We are using the a definition of the coordinate system where the interface is in the xy plane, and the normal to it is in the z direction. We introduce a two-dimensional (2D) coordinate vector $\boldsymbol{\rho}$ in the interface plane with the x and y components only. We assume that the permittivity of the dielectric is a slowly varying function $\varepsilon_d(\boldsymbol{\rho})$. The WKB solution for the in-plane magnetic field is

$$\mathbf{H}(\mathbf{r}, z, t) = \mathbf{H}_0(\mathbf{r}) \exp\left\{[-\kappa(\mathbf{r})|z| + ik_0\phi(\boldsymbol{\rho})] - i\omega t\right\} \ , \tag{3}$$

and κ is the local (at a given $\boldsymbol{\rho}$) value equal to skin-depth exponent κ_m in the metal and evanescent exponent κ_d in the surrounding dielectric (semiconductor). The eikonal $\phi(\boldsymbol{\rho})$ is related to the effective index $n(\boldsymbol{\rho})$ by the standard eikonal equation[48]

$$\left[\frac{\partial \phi(\boldsymbol{\rho})}{\partial \boldsymbol{\rho}}\right]^2 = n^2(\boldsymbol{\rho}) \ . \tag{4}$$

Here, $n(\boldsymbol{\rho})$ is the effective 2D refraction index of SPPs that is locally (at a given $\boldsymbol{\rho}$) given by an expression

$$n(\boldsymbol{\rho}) = \left[\frac{\varepsilon_m(\omega)\varepsilon_d(\boldsymbol{\rho})}{\varepsilon_m(\omega) + \varepsilon_d(\boldsymbol{\rho})}\right]^{\frac{1}{2}} \ . \tag{5}$$

The exponents are given by

$$\kappa_m = k_0 \left[-\frac{\varepsilon_m^2(\omega)}{\varepsilon_m(\omega) + \varepsilon_d(\boldsymbol{\rho})} \right]^{\frac{1}{2}} \quad , \tag{6}$$

$$\kappa_d = k_0 \left[-\frac{\varepsilon_d^2(\boldsymbol{\rho})}{\varepsilon_m(\omega) + \varepsilon_d(\boldsymbol{\rho})} \right]^{\frac{1}{2}} \quad , \tag{7}$$

The surface index $n(\boldsymbol{\rho})$ has a singularity (branch-cut edge) at an SPP stopping point in the complex plane of ω defined by an equation

$$\varepsilon_m(\omega) + \varepsilon_d(\boldsymbol{\rho}) = 0 \ . \tag{8}$$

The real stopping points are given by a related equation

$$\mathrm{Re}\,\varepsilon_m(\omega) + \varepsilon_d(\boldsymbol{\rho}) = 0 \ , \tag{9}$$

beyond which the SPPs do not propagate. This equation in a general case at a given ω defines a line ("caustic") in the plane of ρ where the SPPs are stopped and accumulated.

The adiabatic parameter is defined as the relative change of the SPP wavelength at a distance of this wavelength,

$$\delta = \left| \frac{\partial}{\partial \boldsymbol{\rho}} \frac{1}{k_0 n(\boldsymbol{\rho})} \right| = \left| \frac{1}{k_0 n^2(\boldsymbol{\rho})} \frac{\partial n(\boldsymbol{\rho})}{\partial \boldsymbol{\rho}} \right| \ . \tag{10}$$

For the eikonal approximation to be valid, this adiabatic parameter should be small, which for the conventional optics would be violated at the stopping point. However, for the SPPs at this critical point, δ is finite,

$$\delta = \left| \frac{\partial \varepsilon_d(\boldsymbol{\rho})}{\partial \boldsymbol{\rho}} \middle/ \left(k_0 \varepsilon_m \sqrt{\mathrm{Im}\,\varepsilon_m} \right) \right| \ . \tag{11}$$

Due to this finite value, δ can always be made arbitrarily small by choosing small enough grading $|\partial \varepsilon_d(\boldsymbol{\rho})/\partial \rho|$. In such a case, in contrast to the conventional quantum mechanics of massive particles, the eikonal (WKB) approximation is valid in the *entire* space, including the stopping point and beyond. Mathematically, this is due to the presence of losses that shift the exact stopping point from the real axis into the complex plane. Physically, this means that close to the stopping point, the SPPs accumulate but then they are absorbed, never actually reaching the true singular point where the WKB approximation would have been violated. Close to the stopping point, the group velocity of the SPPs is proportional to the distance to this point; therefore the traveling time to reach this point diverges logarithmically. This is a general properties of the adiabatic nanooptics of the SPPs at interfaces that we will encounter over and over again for various graded plasmonic waveguides described in the this Section below.

The SPP propagation losses decrease with decrease of $\mathrm{Im}\,\varepsilon_m$, which can be achieved by reducing excitation frequency ω. On the other hand, in that region, $|\mathrm{Re}\,\varepsilon_m|$ becomes large. This implies that at the stopping point (9) the required

permittivity of the dielectric is large, $\varepsilon_d = -\mathrm{Re}\,\varepsilon_m = 5 - 15$ for $\omega = 2 - 3$ eV. Such values are typical for semiconductors, e.g., $\mathrm{Al}_x\mathrm{Ga}_{1-x}\mathrm{As}$.[50]
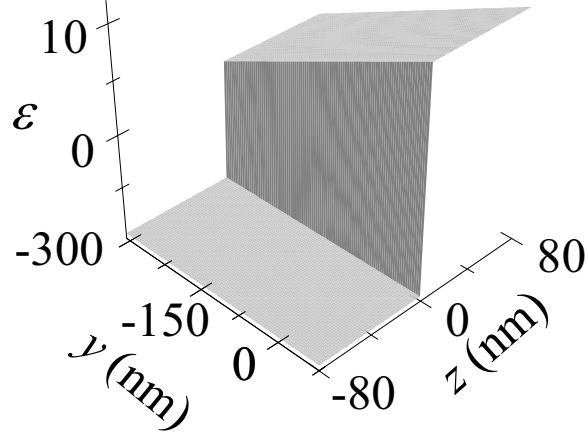

Fig. 1.   Spatial dependence of dielectric constant as a function of coordinates $\boldsymbol{\rho} = (x, y)$ in the xy interface plane.

Below, in numerical illustrations, we set $\omega = 2.5$ eV and reduced vacuum wavelength $\lambdabar = 1/k_0 = 80$ nm. As a metal, we consider silver as having the lowest losses in the optical spectral region.[51] As an example, we consider SPPs propagating along the y direction. Assume that the dielectric (semiconductor) component possesses permittivity with a constant gradient of $\varepsilon_{dy} = \partial\varepsilon_d/\partial y$ in this direction, as illustrated in Fig. 1.

Then the eikonal is a function of only y that be found analytically as

$$\phi(y) = -\frac{1}{\varepsilon_{dy}}\Big\{\, [\varepsilon_d\varepsilon_m(\varepsilon_d + \varepsilon_m)]$$
$$+ \frac{1}{2}\varepsilon_m^{3/2}\ln\left[2\varepsilon_d + \varepsilon_m + 2\varepsilon_d^{1/2}(\varepsilon_d + \varepsilon_m)^{1/2}\right]\Big\}\,, \qquad (12)$$

where $\varepsilon_d = \varepsilon_d(y)$.

The pre-exponential $H_0(\mathbf{r})$ can be found from the conservation of the energy flux utilizing the Pointing vector, which yields

$$H_0 \propto \left(\sqrt{-\varepsilon_m/\varepsilon_d^3} - \sqrt{-\varepsilon_d/\varepsilon_m^3}\right)^{-1/2}. \qquad (13)$$

Close to the stopping point, this pre-exponential becomes large, describing enhancement of the local field by a factor $\sim (|\varepsilon_m|/\varepsilon_1)^{3/4}Q$, where $Q = -\mathrm{Re}\varepsilon_m/\mathrm{Im}\varepsilon_m$ is the quality factor of the SP resonance. This enhancement describes the accumulation of SPP's at the stopping point. An instantaneous solution determined by Eqs. (3)-(13) is shown in Fig. 2, where we can clearly see the stopping of SPP's and the corresponding field enhancement at $y = 0$. Due to the adiabaticity condition, the
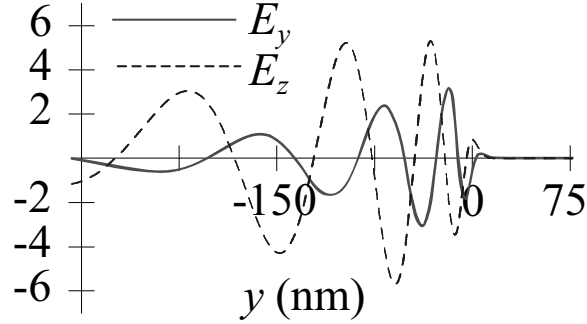
Mark I. Stockman

Fig. 2.   In the vicinity of the stopping point, instantaneous value of optical electric field along the propagation direction y. The solid line is for tangential electric field E_y and the dashed line is for field E_z normal to the interface (the fields are in arbitrary but comparable units).

wave in Fig. 2(a) is not a standing one: it runs from the left to the right, toward the stopping point, where it is not reflected back, but adiabatically stopped, enhanced, and, further in space, absorbed.

The adiabatic parameter should not be too small, otherwise the stopping would be slow and energy losses in the metal high [cf.: for the case of Fig. 2, $\delta \approx 0.1$]. Therefore, this field of phenomena can be called *rapid adiabatic nanooptics*. For the model under consideration, we assume that the dielectric (semiconductor) permittivity is linearly graded at length L of the propagation interval; at the end of this interval $\varepsilon_d = |\varepsilon_m|$. Thus $\partial \varepsilon_d / \partial y \approx |\varepsilon_m|/L$. Taking this into account, from Eq. (12) we find that this rapidity limitation is

$$\delta > \frac{\sqrt{\mathrm{Im}\,\varepsilon_m}}{|\varepsilon_m|} \ . \tag{14}$$

Substituting expression (11) for adiabatic parameter δ and adding the condition of adiabaticity $\delta \ll 1$, we can write a condition on the propagation length L of the SPPs in the adiabatic nanooptics

$$\frac{|\varepsilon_m|}{\mathrm{Im}\,\varepsilon_m} \gtrsim k_0 L \gg \frac{1}{\sqrt{\mathrm{Im}\,\varepsilon_m}} \ . \tag{15}$$

Here the right inequality expresses the condition of adiabaticity, and the left inequality describes the requirement of the rapidity. Note that it is possible to satisfy this double inequality only of the quality factor of the SP resonance is high, i.e., $|\varepsilon_m| \gg \mathrm{Im}\,\varepsilon_m$. We also estimate minimum size l_m of the energy concentration region as $l_m \sim \delta \lambdabar$; it is directly determined by the adiabaticity parameter.

In Fig. 3(a), we show the spatial distribution of local optical intensity I defined as $I(\mathbf{r}) = |\mathbf{E}(\mathbf{r})|^2$, which determines the rates of optical responses of the materials. As the radiation propagates toward the stopping point, the local optical intensity becomes dramatically localized at the metal-semiconductor interface, bound to a layer of hight of < 10 nm at the stopping point ($y = 0$).
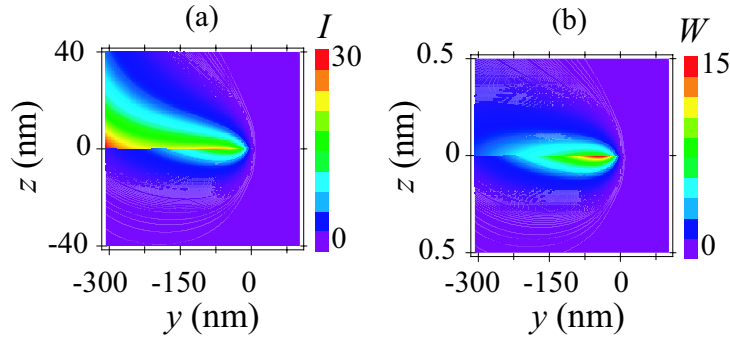
Fig. 3.   For graded dielectric, spatial distributions of the local optical intensity I (a) and optical energy density W (b) (arbitrary units, linear density-coding scales). The distributions are shown in the vertical cross-section (yz) plane.

We display the local optical energy density W

$$W(\mathbf{r}) = \frac{1}{4\pi} \left\{ \mathrm{Re} \, \frac{\partial[\omega\varepsilon(\mathbf{r},\omega)]}{\partial\omega} \, |\mathbf{E}(\mathbf{r},\omega)|^2 + |\mathbf{H}(\mathbf{r},\omega)|^2 \right\} . \tag{16}$$

in Fig. 3(b). The verttical (in yz plane) distribution of the energy is completely different from that of the local field intensity, which is localized mostly in the dielectric (semiconductor) component, except for the vicinity of the stopping point — cf. panel (a). In contrast as panel (b) shows, the energy tends to localize in the metal. The energy density has sharp nanofocus at the stopping point in all three dimensions where it is localized in both the metal and semiconductor components. Thus this graded semiconductor-metal interface system provides an efficient way to delivery the optical energy to nanoscale-size region of high-permittivity semiconductor and metal, which may be useful in applications.

2.3. *General Layered System*

For the sake of convenience and self-containment, we will briefly summarize some results regarding SPPs in layered systems. The problem of the SPP modes in media consisting of metal and dielectric planar layers has been considered by Economou in a pioneering paper.[52] Here we present the corresponding theory in the appropriate detail. We start below with a general layered planar system. In what follows, we will consider a metal film embedded in dielectric.

Consider a general system containing N planar layers of materials with different permittivities. We number these layers by an index $i = 1, 2, \ldots, N$, with the corresponding layer permittivities denoted as ε_i. We position the coordinate system as the following: the xy coordinate plane is parallel to the layers, and the z axis is at the normal to these planes. We will always consider the first layer $(i = 1)$ to be infinite in the direction $z \to -\infty$, and the last layer $(i = N)$ to be infinite in the direction of $z \to \infty$; the thicknesses of the remaining layers we denote as d_i,

$i = 2, \ldots, N-1$. We assume that there exists at least one metal-dielectric interface in this system that supports SPPs.

We seek SPP as a solution of the electromagnetic wave equations that is bound to these layered system and has evanescent behavior in the infinite layers as a transverse magnetic (TM) mode where the magnetic field in an ith layer has only x component and is expressed as

$$H_x^{(i)}(y, z) = \left(A_i e^{\kappa_i z} + B_i e^{-\kappa_i z}\right) e^{iky} \ , \tag{17}$$

where A_i, B_i, κ_i, and k are constants to be determined from equations and boundary conditions. Substituting this in the wave equation, we obtain for each layer,

$$k^2 - \kappa_i^2 = k_0^2 \varepsilon_i \ , \tag{18}$$

where, to remind, $k_0 = \omega/c$.

The sign of κ_i is arbitrary, and we will define it imposing a condition $\mathrm{Re}\,\kappa_i > 0$. Under this sign definition, the condition of the evanescent behavior becomes

$$B_1 = 0 \ , \quad A_N = 0 \ . \tag{19}$$

Exactly as for the case of a single interface, the wave vector k is the same for all the layers as follows from the continuity of H_x at the interfaces. For electric field, the Maxwell curl equation yields

$$E_y = \frac{i}{k_0 \varepsilon_i} \frac{\partial H_x}{\partial z} \ , \tag{20}$$

From this, we obtain the parallel electric field component in an ith layer as

$$E_y^{(i)}(y, z) = \frac{\kappa_i}{\varepsilon_i k_0} \left(A_i e^{\kappa_i z} - B_i e^{-\kappa_i z}\right) e^{iky} \ , \tag{21}$$

and for the normal (transverse) component a general equation is valid:

$$E_y = \mp \frac{i\kappa_i}{k_0 \varepsilon_i} H_x \ , \tag{22}$$

The normal component is given by a general equation

$$E_z = \frac{k}{k_0 \varepsilon_i} H_x \ , \tag{23}$$

form which it follows that it copies the magnetic field.

Now let is determine the number of degrees of freedom (i.e., the difference between the number of unknown variables and the number of independent equations) for the system of equations that we obtain. The Maxwell boundary condition require the continuity of H_x and E_y at each of the $N-1$ interfaces in the system, which supplies $2(N-1)$ equations. Plus, there are N wave equations (18). Thus, overall we have $3N - 2$ equations. Among the unknown variables, there are $2(N-2)$ amplitudes A_i and B_i in the finite layers ($i = 2, \ldots, N-1$), plus two amplitudes (A_1 and B_N) in the semi-infinite layers, plus N evanescent exponents (κ_i), plus the wave vector k. Overall, this sums up to $3N-1$ variables. Subtracting the number $3N-2$

of equations from this, we conclude that there is *one* degree of freedom. This has an absolutely clear meaning. The *linear* system of equations for the amplitudes A_i and B_i, which is obtianed by applying the continuity boundary conditions for fields (17) and (17), does not define the total magnitude of the fields for a SPP mode, but only relative amplitudes. Therefore one of these amplitudes is undetermined, and the rest of them are expressed in terms of that one. This situation is characteristic of any *linear* eigenmode problem.

Eliminating the evanescent exponents κ_i in terms of the wave vector k from the boundary conditions, we obtain a linear system of equations for amplitudes A_i and B_i. For this system to have a nontrivial solution, its determinant should be zero, which gives a characteristic equation for the wavevector k. To be specific, we consider below in this Section a three-layer system where the thickness of the mid layer is d. Carrying out the above-described procedure, we immediately obtain the characteristic equation in a form

$$\exp\left(2k_0\, d\, \varepsilon_2\, u_2\right) = \frac{(u_1 - u_2)(u_3 - u_2)}{(u_1 + u_2)(u_3 + u_2)} \; , \tag{24}$$

where we introduced for each layer a quantity u_i according to the definition

$$u_i = \frac{1}{\varepsilon_i}\sqrt{\left(\frac{k}{k_0}\right)^2 - \varepsilon_i} \equiv \frac{\kappa_i}{k_0\varepsilon_i} \; . \tag{25}$$

Note that Eq. (24) defines a relation between k and ω, where k enters the problem explicitly through coefficients u_i, and ω enters both through parameter k_0 and the frequency dependence of dielectric permittivities ε_i.

By an identity transformation, transcendental Eq. (24) can be given another, equivalent form, which may be more convenient in some analytical or numerical computations,

$$\tanh\left(k_0\, d\, \varepsilon_2\, u_2\right) = -\frac{u_2(u_1 + u_3)}{u_2^2 + u_1 u_3} \; . \tag{26}$$

For the sake of reference, we give the expressions for non-zero coefficients A_i and B_i that define SPP electromagnetic fields:

$$A_1 = 2\exp\left[-\frac{1}{2}k_0 d(u_2\varepsilon_2 + u_3\varepsilon_3)\right]u_2(u_2 - u_3) \; ,$$
$$A_2 = \exp\left[-\frac{1}{2}k_0 d(u_1\varepsilon_1 + u_3\varepsilon_3)\right](u_1 + u_2)(u_2 - u_3) \; ,$$
$$B_2 = \exp\left[-\frac{1}{2}k_0 d(u_1\varepsilon_1 - 2u_2\varepsilon_2 + u_3\varepsilon_3)\right](u_1 + u_2)(u_2 + u_3) \; ,$$
$$B_3 = 2\exp\left[-\frac{1}{2}k_0 d(u_2\varepsilon_2 - u_1\varepsilon_1)\right]u_2(u_1 + u_2) \; , \tag{27}$$

We remind that these equations provide only the relative magnitudes of the coefficients; there is also an undetermined general factor that depends on the intensity and phase of the physical SPP wave.

2.4. *Symmetric Layered system*

There is especial interest in the symmetric three-layer system where the two semi-infinite layers are made of the same material (metal or dielectric), and the middle layer is of a different material (dielectric or metal, respectively). Physically, the special place of such systems is due to the fact the SPP at the two interfaces $1 - 2$ and $2 - 3$ have exactly the same frequency (spectral degeneracy). Therefore they strongly interact and mix (hybridize). The problem solution is facilitated by the appearance of an exact symmetry: parity. With respect to reflection in the plane of symmetry, which we for certainty assume to be at $z = 0$, the fields are either even or odd functions of z. It can be shown that E_z and H_x have always the same parity with respect to the z reflection, and E_y has opposite. It is conventional to associate the parity of a SPP mode with that of E_z. The even SPPs are also often called symmetric, and the odd ones antisymmetric.

For a symmetric system, $\varepsilon_1 = \varepsilon_3$, and the characteristic equation (26) simplifies to acquire a form

$$\tanh\left(k_0\, d\, \varepsilon_2\, u_2\right) = -\frac{2u_1\, u_2}{u_1^2 + u_2^2}\ . \tag{28}$$

To better understand properties of the corresponding solutions and their relation to parity, we re-derive the corresponding characteristic equation from the very beginning using the parity as a good quantum number. Starting with the even (symmetric) SPPs, we impose a specific boundary condition at the symmetry plane $z = 0$,

$$\left. E_y \right|_{z\, =\, 0} = 0\ . \tag{29}$$

After that we only use boundary conditions of the continuity of E_y and H_x at the $1 - 2$ interface (the conditions at the $2 - 3$ interface are redundant), which following the procedure described above in Sec. 2.3 brings about a characteristic equation

$$\tanh\left(\frac{1}{2}\, k_0\, d\, \varepsilon_2\, u_2\right) = -\frac{u_1}{u_2} \tag{30}$$

describing only the even (symmetric) SPPs.

Similar derivation can immediately be effected for the odd SPPs, which satisfy the boundary condition at the symmetry plane

$$\left. H_x \right|_{z\, =\, 0} = 0\ . \tag{31}$$

This leads to the characteristic equation

$$\tanh\left(\frac{1}{2}\, k_0\, d\, \varepsilon_2\, u_2\right) = -\frac{u_2}{u_1}\ , \tag{32}$$

which specifically describes only the odd (antisymmetric) SPP modes.

To compare these defined-parity characteristic equations (30) and (32) with generic Eq. (28), we invoke a hyperbolic trigonometry identity

$$\tanh 2\theta = \frac{2\tanh\theta}{1 + \tanh^2\theta}\ . \tag{33}$$

From this, setting in the left hand side of Eq. (28) $\theta = \frac{1}{2} k_0 \, d \, \varepsilon_2 \, u_2$, we immediately see that the solutions of Eqs. (30) and (32) satisfy Eq. (28) automatically. Thus these two definite-parity characteristic equations together are equivalent to the generic equation (28).

Equivalent characteristic equations with the exponentials in the left-hand sides, which may be more convenient in some cases, are

$$\exp\left(k_0 d u_2 \varepsilon_2\right) = \mp \frac{u_1 - u_2}{u_1 + u_2} \ . \tag{34}$$

The corresponding non-zero coefficients of fields (17), (21), and (23) are

$$A_1 = \pm B_3 = u_2 \ , \quad A_2 = \pm B_2 = \frac{1}{2} \exp\left[\frac{1}{2} k_0 d \left(u_2 \varepsilon_2 - u_1 \varepsilon_1\right)\right] (u_1 + u_2) \ . \tag{35}$$

In these expressions, the upper sign refers to the symmetric SPPs and the lower sign to the antisymmetric SPPs.

2.5. *Adiabatic SPP Concentration in Quasistatic Regime*

In the case of a plasmon polaritonic waveguide whose size (in the direction normal to the SPP propagation) is graded, properties of the adiabatic concentration of optical energy can be described in a quite general form applicable to various waveguide geometries. This is possible due to the fact that in the limit where the SPP reduced wavelength along the propagation direction k^{-1} becomes much smaller than vacuum reduced wavelength $\lambdabar$, the behavior of the SPPs becomes universal. Their wavelength k^{-1} is so small that $\lambdabar$ is irrelevant. In such a case, k^{-1} is determined by and on order of the normal size of the waveguide which is on the nanoscale, i.e., much smaller tham $\lambdabar$. Because $\lambdabar$ disapears from the solution, so does also the speed of light. Hence, the solution becomes quasistatic. All the quantities of the dimensionality of length become on order of normal waveguide size d. Such universality allows one to present a general, universal description based on this scaling.

Consider a plasmon polaritonic waveguide where a SPP can propagate in one dimension (in our convention along the y coordinate) but is restricted in the normal direction by a size, which we assume to be on the nanoscale. For instance, for a metal nanolayer embedded into dielectric or dielectric nanolayer embedded into metal this size is by order of magnitude is the thickness d of the nanolayer and on the same order as the reduced wavelength k^{-1} of the SPPs. A SPP solution for such nanolayers is quasistatic: the magnetic component of the electromagnetic field is much smaller than the electric component.

We consider the thin metal or dielectric layers and similar systems for which there is no cut off: the SPP excitation branch exists for d arbitrarily small (limited, however, by Landau damping to $d \gtrsim v_F/\omega$). Then the properties of the adiabatic concentration can be established in a quite general form.

We will consider systems where the dielectric losses of the SPPs are not too large. Then in the first approximation, the energy of the SPPs is conserved, and so should

Mark I. Stockman

be its total flux. In what follows, we will not be interested in specific coefficients but will trace only the scaling with the layer thickness d. The conservation of energy is reflected in the conservation of the energy flux as

$$v_g \int \mathbf{E}^2 \mathrm{d}xz = \mathrm{const} \ , \tag{36}$$

where we remind that v_g is the group velocity. Because the only relevant parameter of the problem with the dimensionality of length is d (the radiation vacuum wavelength is many orders of magnitude too large), then the group velocity asymptotically (for nano-thin systems) scales as

$$v_g \propto d \ . \tag{37}$$

We will consider two type of systems: (i) thin layers, which provide one-dimensional (1d) confinement of the fields, and (ii) cones or prisms, which provide the pwo-dimensional (2d) confinement. Correspondingly, the integral in Eq. (36) can be estimated as $|E|^2 d^\nu$, where $\nu = 1, 2$ is dimensionality of the waveguide, as discussed above. From this, taking (36) and (37) into account, we obtain the scaling of the electric field inside the polaritonic waveguide with its characteristic size d as

$$E \propto d^{-\frac{1+\nu}{2}} \ . \tag{38}$$

The wave propagation in the WKB approximation is described by the eikonal $\phi = \int k(y) \, \mathrm{d}y$, where $k(y)$ is the wave vector at the coordinate y along the waveguide. The universal quasistatic scaling for the nano-thin waveguides implies that k is inversely proportional to the only relevant parameter of the problem with the dimensionality of length, which is d, i.e.,

$$k(y) = \frac{k_a}{d(y)} \ , \tag{39}$$

where k_a is a complex constant, and $d(y)$ is the waveguide grading, i.e., the dependence of its thickness on the longitudinal coordinate y. As a result, both the phase velocity and group velocity of the SPPs scale with nanolayer thickness as

$$v_p = \frac{\omega}{\mathrm{Re}\, k_a} d \ , \quad v_g = \left(\frac{\partial \mathrm{Re}\, k_a}{\partial \omega} \right)^{-1} d \ . \tag{40}$$

This scaling along with Eq. (38) brings about the dependence of the field along the waveguide as

$$|E| \propto d^{-\frac{1+\nu}{2}} \exp\left[-\mathrm{Im}\, k_a \int \frac{\mathrm{d}y}{d(y)} \right] \ . \tag{41}$$

Assuming for simplicity a constant grading of the waveguide, $d' = \partial d / \partial y = \mathrm{const}$,

$$|E| \propto d^{-\frac{1+\nu}{2} - \frac{\mathrm{Im}\, k_a}{d'}} \ . \tag{42}$$

This is a very general result that follows from scaling properties of the quasistatic solution. Interestingly enough, it shows that the field increases along the waveguide if the grading exceeds a certain critical value,

$$-d' > 2\frac{\operatorname{Im} k_a}{1 + \nu} \ . \tag{43}$$

From Eq. (42), it follows that field intensity I and energy density W also asymptotically obey a universal scaling

$$I \propto W \propto d^{-(1+\nu)-2\frac{\operatorname{Im} k_a}{d'}} \ . \tag{44}$$

Note that $-d' > 0$, and that the the adiabatic parameter

$$\delta = |\frac{d(k^{-1})}{dy}| = \frac{1}{k_a}|d'| \ . \tag{45}$$

This parameter is finite along the entire waveguide including its apex. Thus the WKB can be applicable for the entire system, in contrast to the quantum mechanics where it is violated at the stopping (turning) points. It is important to understand how this situation can take place. The answer is in the travel time needed for the SPPs to reach the apex that plays the role of such a stopping point. This travel time T_t for SPPs at an initial coordinate point y_i to the final coordinate point y_f is

$$T_t = \int_{y_i}^{y_f} \frac{\mathrm{d}y}{v_g} \propto \ln \frac{y_i}{y_f} \ , \tag{46}$$

where we took into account scaling (37) and assumed for simplicity a constant grading, i.e., $d' = \text{const}$. It is obvious that T_t logarithmically diverges for $y_f \to 0$. This implies that it takes SPPs infinite time to travel to the apex, which is a singular point. This is the underlying reason why the WKB solution is valid for the entire waveguide.

Because k_a is a (complex) constant whose modulus is on order of 1 [see, e.g., Eq. (48)], the adiabaticity condition $\delta \ll 1$ reduces to $|d'| \ll 1$. We aslo see that in this asymptotic regime, the adiabatic parameter is always finite. Also, the "'best" solution is such that the adiabatic parameter is as large as possible compatible with the adiabaticity, because it minimizes the propagation time and, correspondingly, the dielectric losses. But this also implies that this parameter should be constant in the asymptotic region ($k \sim d^{-1} \gg k_0$); the grading, correspondingly, should also be constant, $d' = \text{const}$.

For the graded waveguide in the shape of a wedge or a cone, $-d' = \tan\theta$, where θ is the angle at the tip of this wedge or cone. Thus condition (43) shows that the grade angle θ of the waveguide should be large enough,

$$\theta > \theta_{min} = \arctan\left(2\frac{\operatorname{Im} k_a}{1 + \nu}\right) \ . \tag{47}$$

If condition (43) or (47) is violated, then the fields in the waveguide will monotonously decay along the waveguide. If the losses in the waveguide are large, this inequality or (43) may contradict to the adiabaticity condition $|d'| \ll 1$.
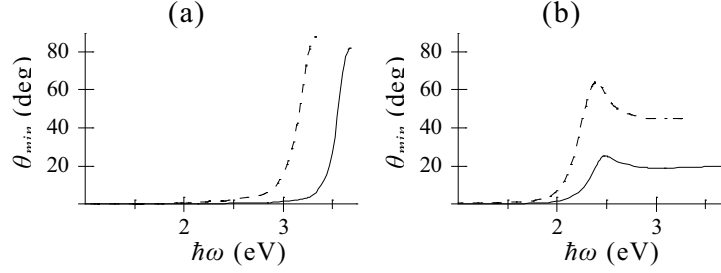
Fig. 4.   Minimum grading angle θ_{min} (degree) at which the adiabatic concentration causes increase of SPP field toward the tip of the plasmon polaritonic waveguide. This angle is displayed as a function of the SPP frequency (eV). The calculations are applicable to a wedge-shaped nanolayer of metal in dielectric or dielectric nano-wedge in metal. The metal is silver (a) and gold (b). Dielectric permittivity $\varepsilon_d = 1$ (solid curves) and $\varepsilon_d = 3$ (dashed curve). Each curve is shown within the spectral range of the existence of the corresponding SPP mode, i.e., for $\omega \leq \omega_{sp}$.

The value of k_a depends on the specific model. For instance, for a nano-thin metal layer in dielectric environment or nanolayer of dielectric embedded in a metal, we obtain

$$k_a = \ln \left[\frac{\varepsilon_m(\omega) - \varepsilon_d}{\varepsilon_m(\omega) + \varepsilon_d} \right] \; . \tag{48}$$

This expression is valid for the symmetric SPPs in the case of the dielectric nanolayer in metal and for the antisymmetric SPPs for the case of the metal nanolayer in dielectric (the modes of the opposite symmetry in each of these two cases are highly lossy and will not be considered). Note that because $\mathrm{Re}\,\varepsilon_m + \varepsilon_d < 0$, the real part of the argument of the logarithmic function is positive. Therefore, $\mathrm{Im}\,k_a$ originates only from the existence of $\mathrm{Im}\,\varepsilon_m$, i.e., from the dielectric losses in the metal, which is natural to expect.

We show in Fig. 4 dependence of minimum angle $\theta_m in$ on frequency of SPPs for both vacuum and a dielectric with $\varepsilon_d = 3$ for silver and gold as a metal. To remind, the adiabaticity condition requires $\tan \theta_{min} \ll 1$, so the value of θ_{min} should not be large. One can reasonable assume that a value acceptable from the requirements of adiabaticity is $\theta_{min} \lesssim 20$ deg. This is satisfied for silver in wide frequency range of the near-ir and entire visible spectrum, $\hbar\omega \leq 3.1$ eV; for vacuum this condition is actually more relaxed. In contrast, for gold the adiabaticity requirement is stronger, leading to $\hbar\omega \leq 2.1 eV$, thus limiting to the near-ir and red-yellow spectral region. The reason for this difference is the ds band absorption in gold that is in the green-blue spectral region, while for silver it is in the near uv.

Let us note that formally the results presented above are valid for all types of SPPs in symmetric planar waveguides: even or odd. However, in the region of high k, the frequencies of the even (symmetric) modes for the metal nanolayer guide and of the odd (antisymmetric) modes for the dielectric nanolayer guide are high, leading to high losses and, correspondingly, to large values of θ_{min} that contradict to the adiabaticity. Thus, the results presented above in this Section are valid for
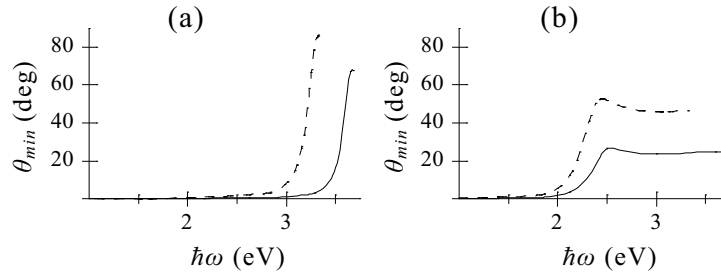
Fig. 5.   The same as in Fig. 4 but for nanocone as a SPP waveguide, for TM_0 mode. Angle θ in this case is an angle between the cone axis and its surface.

and applicable to the lower frequency SPP modes. These "good" modes are the odd (antisymmetric) SPPs in the metal nanolayers and the even (symmetric) modes in the dielectric nanolayer in the metal waveguides.

Another system of interest is a metal conical (tapered cylinder) waveguide introduced in Ref. 10 — see also Sec. 2.7. In this case, as a measure of the transverse size of the waveguide d we choose the local cone radius R that depends on the longitudinal (along the propagation direction) coordinate z. The formulas given above in this Section apply with the substitution $d \to R$ and for $\nu = 2$. However, the value of coefficient k_a for a TM_0 SPP mode in a tapered cylinder changes to[10]

$$k_a = 2 \left\{ \frac{\varepsilon_d}{\varepsilon_m(\omega)} \frac{1}{\ln\left[\frac{\varepsilon_d}{4\varepsilon_m(\omega)}\right] + 2\gamma} \right\}^{1/2} , \qquad (49)$$

where $\gamma \approx 0.577216$ is the Euler constant. Note that this analytical expression is an approximation valid in the long-wavelength portion of the optical spectrum where $-\varepsilon_m(\omega) \gg \varepsilon_d$.

Using this function in Eq. 47, we have obtained the spectral dependence of minimum angle θ_{min} for which the adiabatic increase of the SPP field intensity in the direction of the cone tip will take place. For smaller angles, the linear losses in the metal will overcome the adiabatic concentration and the SPP intensity will monotoneously decrease along the cone. Such dependences for silver and gold are displayed in Fig. 5.

First, we note that these dependences for the nanocone are remarkably similar, practically identical to the corresponding dependences for metal nanowedges — cf. Fig. 4. This is despite the fact that the underlying coefficients k_a, which solely define these spectral dependences, are utterly different by form — cf. Eqs. (48) and (49). Take into account, however, that angle θ_{min} in Eq. (48) is the full angle at the tip of the wedge, while in Eq. (49) it is the angle between the cone axis and its surface, i.e., the half of the full constituent angle at the tip of the cone.

Returning to Fig. 5, for the case of the cone, the same as for the wedge, the silver provides much better a system where the plasmonic concentration can be expected

for smaller angles in a wider spectral range. For gold, the required minimum angle increases dramatically toward the 2.2 eV edge of the *ds* band absorption, which dramatically limits its usefulness. Note that large required angles contradict to the adiabaticity requirement $\tan\theta \ll 1$.

In conclusion of this Section, we discuss the limits of the adiabatic energy concentration in SPP waveguides. The optical losses, as we discussed above is the most important limiting factor within the macroscopic local electrodynamics that limits the efficiency of the energy delivery to the nanoscale. It also limits the minimum angle for which the field enhancement at the tip of the waveguide occurs and can make the adiabatic regime unattainable whatsoever — see the discussion of Eqs. (48) and (49). Important limiting effects that become important at the small scale are the spatial dispersion of the dielectric responses and Landau damping. These effects are described by spatially dispersive, nonlocal dielectric function. Though there has been some work done on the nonlocal effects in the adiabatic SPP concentration,[53] this area is still mostly unexplored.

On a qualitative level, the nonlocality of the dielectric responses and Landau damping become important when the localization size of the SPPs becomes on order of the correlation length associated with the Fermi velocity v_f of electrons. Because in the adiabatic following regime, this localization length is on order of local size d of the waveguide, then the condition that these effects are important is

$$d \sim k^{-1} \lesssim v_f/\omega \ . \tag{50}$$

In practical terms, in the optical region the effects of Landau damping and dielectric nonlocality become important for d of order of a few nanometers. This critical size increases when the frequency decreases toward the red and infrared spectral region.

There are also other phenomena limiting the adiabatic energy concentration on the nanoscale, which become important when the size of the waveguide d becomes very small, that can only be described in a fully microscopic theory. These are electron spill out and the related underscreening. These effects have recently been considered for the problem of the surface enhanced Raman scattering (SERS) in the framework of the local density approximation (LDA) of the density functional theory (DFT).[54–58] The application of this or other microscopic methods to the problem of the adiabatic transformation and concentration of the optical energy on the nanoscale is still ahead.

2.6. *Adiabatic SPP Stopping in Metal Wedge*

In this Section we consider the adiabatic transformation and concentration of energy in a metal wedge embedded in dielectric media. We start with a symmetric problem: the embedding dielectric is uniform. In this case, the SPP modes are characterized by parity. Inspection of the corresponding dispersion relations for the even (symmetric) and odd (antisymmetric) SPPs (30) and (32) shows that it is the antysymmetric mode that has velocity that decreases when the layer becomes
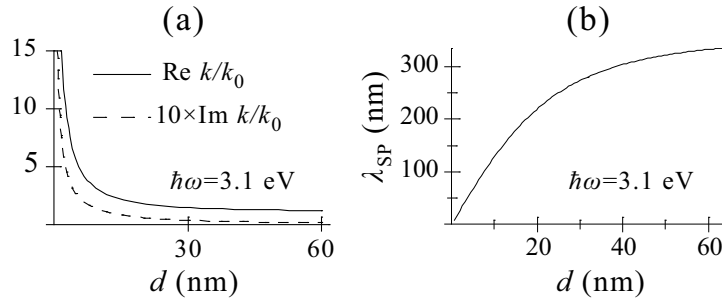
Fig. 6.   (a) For a silver nanofilm in vacuum, dependence of the real part of the SPP effective refraction index, $\mathrm{Re}\, k/k_0$, on the layer thickness d (solid line). The same dependence for the imaginary part of the SPP index, $\mathrm{Im}\, k/k_0$, is displayed by the dashed line multiplied by a factor of 10. (b) Dependence of the SPP wavelength, $\lambda_{SP} = 2\pi/\mathrm{Re}\, k$. The dependences are calculated for the antisymmetric mode of frequency $\omega = 3.1$ eV.

thin, which is the prerequisite for the adiabatic following by the SPPs of the layer thickness.

Correspondingly, the starting point of our consideration is the characteristic equation for the antisymmetric SPPs (32). It provides the antisymmetric SPP dispersion relation as a complex function $k(\omega, d)$ of frequency and the metal layer thickness. As an example, we show in Fig. 6 (a) the dependence of the wavevector on the layer thickness for a silver nanolayer in vacuum. Note that the ratio $n = k/k_0$ that is shown in the graphs is the effective refraction index for the antisymmteric SPPs. As we see from this figure, both the real and imaginary part of this effective index increas when the layer thickness is in nanometer range and decreases. As we know from the general scaling theory of the adiabatic following presented above in Sec. 2.5, this dependence is $n \propto 1/a$ — see Eq. (39). This scaling should take place for the local wedge thickness less or on order of the skin depth in the metal, $d \lesssim l_s \sim 20$ nm. Such a behavior is actually in a very good agreement with the curves in Fig. 6.

The imaginary part of the wavevector, as we see from Fig. 6 (a) is small relative to its real part, $\mathrm{Im}\, k/\mathrm{Re}\, k \lesssim \frac{1}{20} - \frac{1}{30}$. Thus the antisymmetric SPPs remain good propagating waves for even for very thin nanolayers. This relatively weak decay and their high index makes them useful for ultramicroscopy. The resolution (both in-plane and out-of-plane) that can be obtain with such modes is determined by their wavelength λ_{SP} displayed in Fig. 6 (b). For instance, for the wedge tapered down to 4 nm, $\lambda_{SP} \approx 30$ nm, which is in agreement with the scaling of their reduced wave length $\lambdabar_{SP} \sim d/k_a \sim d$. The corresponding resolution is ~ 15 nm. It is sometimes called an "X-ray resolution at optical frequencies".

From the dispersion relation, one can calculated the phase velocity and group velocity of the SPP. They are shown in Fig. 7 (a) as function of the nanolayer thickness. The phase velocity for relatively thick nanolayers ($d \ll l_s$) is close to speed of light, while the group velocity is significantly less than that. For thin
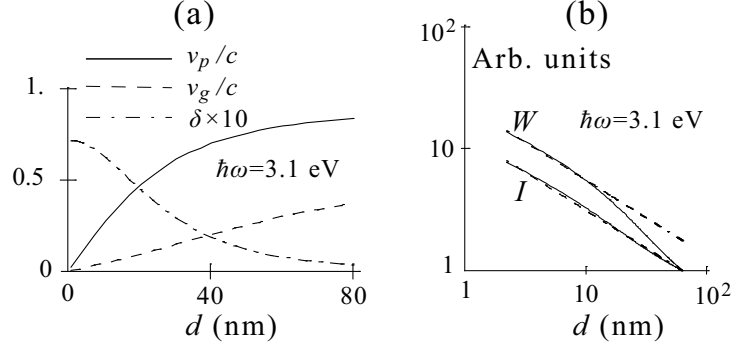
Fig. 7.   (a) For silver wedge in vacuum, displayed as functions of wedge local thickness d plotted are: phase velocity v_p (solid curve), group velocity v_g (dashed curve), and adiabatic parameter δ multiplied by a factor of 10 (dash-dot curve); (b) Dependences of intensity I on the vacuum side of the silver surface and energy density W on its metal side as a function of the wedge local thickness d. The results of WKB theory are shown by solid lines, and those of the scaling approximation are denoted by the dashed lines. Note the double logarithmic scale.

nanolayers ($d \lesssim l_s$), both these velocities tend to zero proportionally d, in accord with the general scaling (40). Thus, the adiabatic following of the nanolayer by the SPPs provides an efficient (with relatively low losses) wide-band approach to obtaining the "slow light".

The adiabatic parameter δ (multiplied for the sake of the readability by a factor of 10) is also shown in Fig. 7 (a). It is finite in the entire region of propagation, including the vicinity of the stopping edge, in acord with the scaling law (45). This examples uses grading of the wage $d' = -1/30$. For this value of grading, the WKB parameter is small even at the edge, $\delta \leq 0.07$. Correspondingly, the WKB approximation is valid for the entire system.

Now let us consider the fields. The WKB solutions can be obtained from the exact expressions by multiplying them by the corresponding exponential of the eikonal, $\exp(i\phi)$ and a pre-exponential $\propto J^{-1/2}$, where J is the energy flux that allows one to satisfy the energy conservation condition. We give below the corresponding expressions explicitly in the general case, without assuming that the system is symmetric. For layer 1, which is the semiinfinite ($z < 0$) dielectric underlying the metal wedge, we have

$$H_x^{(1)} = \frac{1}{\sqrt{J}} A_1 \exp\left[\kappa_1 z + i\phi(y)\right] ,$$

$$E_z^{(1)} = \frac{1}{\sqrt{J}} \frac{k}{k_0 \varepsilon_1} A_1 \exp\left[\kappa_1 z + i\phi(y)\right] ,$$

$$E_y^{(1)} = \frac{1}{\sqrt{J}} \frac{\kappa_1}{k_0 \varepsilon_1} A_1 \exp\left[\kappa_1 z + i\phi(y)\right] , \tag{51}$$

where eikonal

$$\phi(y) = \int k(d(y))\mathrm{d}y , \tag{52}$$

and $k = k(d)$ is a function of the local thickness d, and so is $\kappa_1 = \kappa_1(d)$ as given by the general relation (18), where, by definition, $k_0 = \omega/c$.

For layer 2, i.e., the metal wedge $d(y) \geq z \geq 0$, the solutions are

$$H_x^{(2)} = \frac{1}{\sqrt{J}} \left[A_2 \exp\left(\kappa_2 z\right) + B_2 \exp\left(-\kappa_2 z\right) \right] \exp\left[i\phi(y)\right] ,$$

$$E_z^{(2)} = \frac{1}{\sqrt{J}} \frac{k}{k_0 \varepsilon_2} \left[A_2 \exp\left(\kappa_2 z\right) + B_2 \exp\left(-\kappa_2 z\right) \right] \exp\left[i\phi(y)\right] ,$$

$$E_y^{(2)} = \frac{1}{\sqrt{J}} \frac{\kappa_2}{k_0 \varepsilon_2} \left[A_2 \exp\left(\kappa_2 z\right) - B_2 \exp\left(-\kappa_2 z\right) \right] \exp\left[i\phi(y)\right] . \tag{53}$$

Finally, the fields for the semi-infinite upper dielectric layer 3 ($z > d(y)$) are

$$H_x^{(3)} = \frac{1}{\sqrt{J}} B_3 \exp\left[-\kappa_2 z + i\phi(y)\right] ,$$

$$E_z^{(3)} = \frac{1}{\sqrt{J}} \frac{k}{k_0 \varepsilon_1} B_3 \exp\left[-\kappa_3 z + i\phi(y)\right] ,$$

$$E_y^{(3)} = \frac{1}{\sqrt{J}} \frac{\kappa_3}{k_0 \varepsilon_3} B_3 \exp\left[-\kappa_3 z + i\phi(y)\right] , \tag{54}$$

The coefficients of these equations can be found in general case, but they are cumbersome and we do not display them.

The WKB recipe to find the pre-exponential $1/\sqrt{J}$ is the following. At the first stage one neglects the imaginary part of the eikonal. Fields (51)-(54) should then be used to compute the energy density (16). Finally, energy flux J, which determines the pre-exponential, is computed as

$$J(y) = v_g \int_{-\infty}^{\infty} W(y, z)\mathrm{d}z . \tag{55}$$

As everywhere, $v_g = \partial\omega/\partial k$ is the group velocity [see a numerical illustration in Fig. 7 (a)], which depends on the local thickness $d = d(y)$.

As a result of elementary but bulky computations, we obtain

$$J = v_g \left\{ \frac{k_0 |A_1|^2}{2\mathrm{Re}\,\kappa_1} \left(1 + \frac{|k|^2 + |\kappa_1|^2}{k_0^2 \varepsilon_1} \right) + \right.$$

$$\frac{k_0}{2\mathrm{Re}\,\kappa_2} \left[1 + \mathrm{Re}\left(\frac{\partial\omega\varepsilon_2(\omega)}{\partial\omega} \right) \frac{|k|^2 + |\kappa_2|^2}{k_0^2 \varepsilon_2} \right] \times$$

$$\left\{ |A_2|^2 \left[\exp\left(2\mathrm{Re}\,\kappa_2 d\right) - 1 \right] + B_2|^2 \left[1 - \exp\left(-2\mathrm{Re}\,\kappa_2 d\right) \right] \right\} +$$

$$\frac{k_0}{\mathrm{Im}\,\kappa_2} \mathrm{Re}\left(\frac{\partial\omega\varepsilon_2(\omega)}{\partial\omega} \right) \frac{|k|^2 - |\kappa_2|^2}{\left|k_0^2 \varepsilon_2\right|^2} \mathrm{Im}\left\{ AB^* \left[\exp\left(2i\mathrm{Im}\,\kappa_2 d\right) - 1 \right] \right\} +$$

$$\left. \frac{k_0 |B_3|^2}{2\mathrm{Re}\,\kappa_3} \left(1 + \frac{|k|^2 + |\kappa_3|^2}{k_0^2 \varepsilon_3} \right) \left[1 - \exp\left(-2\mathrm{Re}\,\kappa_3 d\right) \right] \right\} . \tag{56}$$

Substituting this into the expressions for fields (51)-(54) and computing eikonal (52) by numerical integration, we obtain the required WKB solution. Note that the
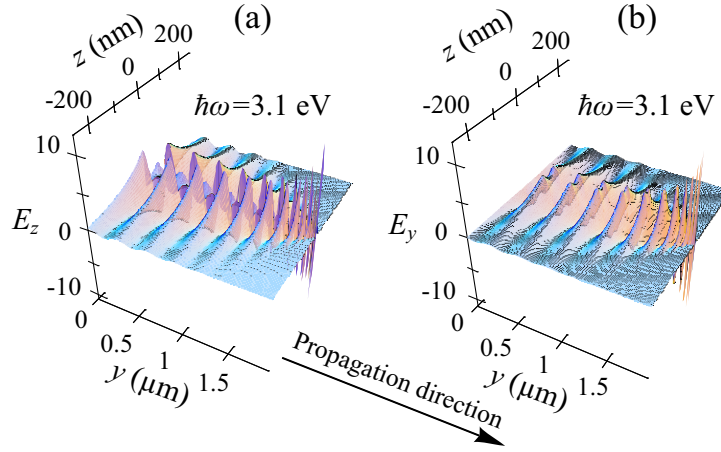
Mark I. Stockman

Fig. 8.   Local electric fields of SPP antisymmetric mode with frequency $\omega = 3.1$ eV where panel (a) displays normal field E_z, and panel (b) shows the longitudinal field E_y. The wedge material is silver, and the embedding medium is vacuum. The wedge's slope tangent is $\tan\theta = 1/30$.

fields (51)-(54) should be multiplied by a common normalization multiplier that defines the energy of a specific solution.

Returning back to Fig. 7 (b), we compare the local field intensity I and energy density W of an SPP mode obtained from this solution with the scaling prediction (44) for a silver nanowedge with grading $d' = -1/30$, which is well over the critical value needed for the adiabatic concentration to take place. The only adjustable parameter in such a comparison is the mode normalization coefficient mentioned above in the previous paragraph. Note that these quantities are displayed as functions of the local metal wedge thickness d. The scaling agreement is very good for W in the asymptotic region, i.e. for d significantly less than skin depth $l_s \approx 25$ nm of the metal, as expected. What is surprising, the local intensity on the outside surface of the metal scales almost perfectly in the entire region.

The distributions of the local electric fields in the plane normal to wedge surface in the direction of propagation is shown in Fig. 8 for a silver nanowedge with $d' = -1/30$. These distributions demonstrate well the general qualitative properties of the adiabatic transformation and concentration of energy on the nanoscale. For the wedge thickness large enough, $d \gg l_s$, which is the case in the left-hand side of the panels, the fields are delocalized outside the metal at distances greater than the wavelength in vacuum; the normal field, E_z, inside the metal is weak. This behavior is similar to skin effect in a semi-infinite metal. In this region, the SPP wavelength in the direction of propagation is smaller than the vacuum wavelength but still is on the microscale rather than on the nanoscale. As the SPPs propagate toward the edge (to the right in the figure), the local thickness of the wedge becomes comparable with the skin depth, and then the adiabatic following sets on. Both the wavelength in the propagation direction and the evanescent length at the normal to
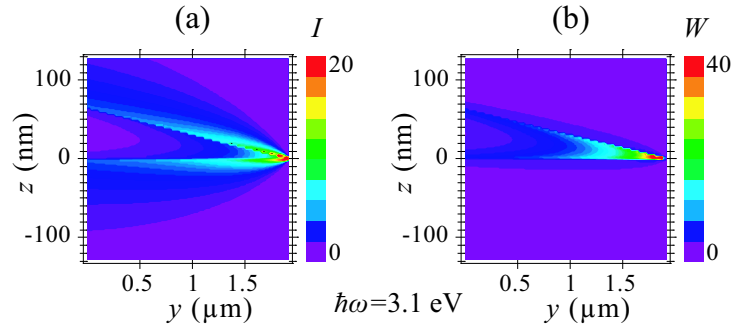
Fig. 9.   For antisymmetric SPP mode of silver wedge in vacuum, distributions in the normal plane of propagation (yz) of local field intensity I (a) and energy density W (b). Frequency is $\omega = 3.1$ eV, wedge material is silver. Color coding bars are shown to the right of the plots along with the corresponding scales.

the surface become on order of the local wedge thickness. This nanolocalization is accompanied by a sharp increase in the amplitude of the fields as the SPP approach the edge in the right-hand side of the panels. Also, in this region, the skin effect becomes inefficient: the entire thickness of the metal is filled with the fields.

   Now let us turn to the spatial distribution of the local electric field intensity defined here as

$$I(y, z) = |E_z(y, z)|^2 + |E_y(y, z)|^2 . \tag{57}$$

This distribution in the plane of propagation normal to the interfaces (the yz plane) is displayed in Fig. 9 (a). Here we can clearly see that at the widest part of the wedge, where its thickness significantly exceeds the skin depth, the fields are delocalized in the normal plane at micrometer-scale distances. The thin skin layers at the surfaces and low field area in the middle of the wedge are clearly evident. As the SPPs propagate toward the edge (to the right in the figure), their fields become more localized at teh surfaces and start to penetrate the bulk of the metal. When the adiabatic following is fully developed (for $y \gtrsim 1.5\mu$m), the entire cross section of the metal is uniformly filled with the fields and their localization length outside of the metal is comparable with the local thickness of the wedge. This is in the full qualitative agreement with the picture produced by the scaling theory — see Sect. 2.5. In the process of propagation toward the edge, the intensity at the outer surface of the metal (where it is maximum) is increased by a factor of ~ 10 [corresponding to the change of the coding (false) color in the plot from light blue to intense red].

   Consider the adiabatic concentration of energy density $W(y, z)$ (16) illustrated in Fig. 9 (b). In contrast to the intensity that is mostly localized in the dielctric component (vacuum in this case) [cf. panel (a)], the energy density is much more concentrated in the metal due to the high magnitude of the metal dielectric permittivity. When the SPPs propagate toward the sharp wedge, the metal wedge becomes uniformly filled with the electromagnetic energy density. Toward the wedge, within

Mark I. Stockman

the range of the plot, the energy density increases by more than a factor of 10. Thus the metal wedge is an efficient conductor and adiabatic concentrator of the SPP energy.

It is of interest to evaluate qualitatively what is the fraction of the electromagnetic energy flux propagating in the metal (to be denoted below as J_m) with respect to that propagating in the dielectric (to be denoted as J_d). It is most interesting and also easiest to do in the quasistatic regime (for this specific plot, such a regime is established for $y \gtrsim 1~\mu\mathrm{m}$).

In the quasistatic regime, the field coefficients can be found in a simplified form. From these, we immediately obtain expressions for the electric fields (the magnetic field in the quasistatic regime is small by parameter k_0/k and can be neglected). For the embedding dielectric, we obtain

$$E_z(y, z) = E_y(y, z) = \pm\varepsilon_m \exp\left[-k|z| + i\phi(y)\right] , \tag{58}$$

where signs $\pm$ refer to the upper and lower half spaces. For the metal wedge, we obtain

$$E_z(y, z) = (\varepsilon_d + \varepsilon_m)\sinh(kz)\exp\left[i\phi(y)\right] ,$$
$$E_y(y, z) = (\varepsilon_d + \varepsilon_m)\cosh(kz)\exp\left[i\phi(y)\right] . \tag{59}$$

Reminding again, there is an arbitrary normalization coefficient that these eigenmode fields should be multiplied by to obtain observable, physical fields, which defined the total phase and intensity of the SPP.

With these fields, it is easy to find the ratio of the electromagnetic energy fluxes in the metal and dielectric

$$\frac{J_m}{J_d} = \frac{\int_0^{d/2} W(y, z)\mathrm{d}z}{\int_0^{\infty} W(y, z)\mathrm{d}z} . \tag{60}$$

Computing this ratio, one can safely neglect a small imaginary part of the metal dielectric function. We obtain a simple, closed expression

$$\frac{J_m}{J_d} = -\frac{1}{\varepsilon_m}\frac{\partial\left[\omega\varepsilon(\omega)\right]}{\partial\omega}\frac{(\varepsilon_d + \varepsilon_m)^2}{(\varepsilon_d - \varepsilon_m)^2} . \tag{61}$$

Note that this ratio does not depend on local thickness d of the wedge, as expected in the asymptotic quasielectrostatic regime. Numerical evaluation of this ratio for the present system shows that in the entire plasmonic range, between 1 and 3 eV, this ratio varies very little, just between 0.9 and 1.6. Thus, the electromagnetic (or, rather, quasielectrostatic) energy is split approximately equally between the metal and dielectric components of the plasmonic waveguide. Note that typically in the plasmonic region $|\varepsilon_m| \gg \varepsilon_d$. In such a case, Eq. (61) further simplifies

$$\frac{J_m}{J_d} = -\frac{1}{\varepsilon_m}\frac{\partial\left[\omega\varepsilon(\omega)\right]}{\partial\omega} . \tag{62}$$

This expression does not depend on the dielectric at all, and it is numerically very close to 1 for silver.
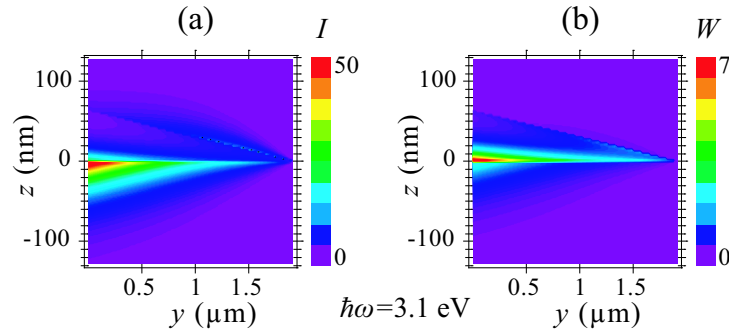
Fig. 10.   Same as in Fig. 9 but for an asymmetric nanowedge SPP waveguide: $\varepsilon_1 = 3$, and $\varepsilon_3 = 1$.

Returning to Fig. 9 (b), we note that the graphics renditions visually overestimates the fraction of the optical energy propagating in the metal, which appears to be significantly greater than 1. This is due to the fact that the dielectric fields are spread over the two (upper and lower) semi-infinite dielectric regions, and also in both of these regions they are delocalized somewhat greater than the fields in the metal. In teh actuality, as we know from Eqs. (61) and (62), the SPP optical energy in the quasielectrostatic regime propagates in approximately equally fractions in the metal and dielectric constituents of the waveguide.

Finally, it is of significant interest to consider an asymmetric SPP waveguide constituted by a metal wedge surrounded on both sides by different dielectrics. In particular, this is a case for the metal wedge on a dielectric substrate surrounded by vacuum.

Qualitatively, the underlying physics of the SPP adiabatic energy transformation and concentration is somewhat different from the symmetric case. In the present case, for a thick ($d \gg l_s$) portion of the wedge, the SPP propagating at the lower and upper interfaces for the same ω have different wave vectors and very weakly interact and hybridize with each other (i.e., it is a case of weak coupling). The situation changes for $d \lesssim l_s$ when the coupling and mixing of the SPPs at both the interfaces become strong. In this case, we select the high-k mode that is asymptotically (for a very strong coupling) antisymmetric, slow SPP branch. This one provides the best adiabatic control and concentration of energy.

The distribution of the local field intensity for such a slow SPP mode in the normal plane of propagation (the yz plane) is illustrated in Fig. 10 (a) for $\varepsilon_1 = 3$ (a typical glass), $\varepsilon_3 = 1$ (vacuum), and silver as the metal. As we see from the figure, the mode selected is initially (in the left-hand side of the figure) localized predominantly at the lower (metal/dielectric) interface and is mostly a SPP at the interface of the semi-infinite silver and the dielectric (glass). As it propagates to the right (toward the edge) it does become much more concentrated in space with the localization length on order of a few nanometers. However, this localization is not accompanied by an enhancement in its intensity. In fact, this intensity decays

by a factor of ~ 10 due to the losses. This is due to the much smaller component of the adiabatically-controlled odd mode in this SPP because of the much weaker coupling between the two interfaces.

The behavior of the optical energy density in this system is illustrated in Fig. 10 (b). In contrast to panel (a), the energy is much more concentrated in the metal, similar to what takes place for the symmetric wedge waveguide discussed above in conjunction with Fig. 9. The energy density actually decays significantly less than the local field intensity due to its better localization: along the propagation pass it is attenuated only by a factor of ≈ 3. Thus even an asymmetric SPP waveguide is an efficient adiabatic concentrator of optical energy.

2.7. *Adiabatic Concentration and Stopping of SPPs in Tapered Nanoplasmonic Cylinder*

Consider a nanoplasmonic waveguide that consists of a metal nanowire whose axis coincides with the coordinate z axis and whose dielectric function $\varepsilon_m(\omega)$ is uniform in space, where ω is the optical excitation frequency. The radius $R(z)$ of this nanowire is a smooth function of z and is assumed to decrease from microscale for z large negative to a nanoscale size at $z \to 0$, as discussed above, see Fig. 11(a). This wire is surrounded by a dielectric medium with dielectric constant ε_d. Using the smoothness of dependence $R(z)$, we will employ the eikonal approximation[48] also called Wentzel-Kramers-Brillouin (WKB) or quasiclassical approximation in quantum mechanics.[49]

We consider an axially uniform SPP mode that is a TM wave whose magnetic field has the ϕ polarization, and electric field **E** has both transverse (radial) component E_r and longitudinal component E_z. In the eikonal (WKB) approximation, this field has the form

$$\mathbf{E}(\mathbf{r}, z, t) = \mathbf{E}_0(\mathbf{r})A(z)\exp[ik_0\varphi(\mathbf{r}) - i\omega t] \qquad (63)$$

where **r** is a two-dimensional (2D) vector in the xy plane, $k_0 = 1/\lambdabar$, and $A(z)$ is a slow-varying pre-exponential factor, to be determined later in this Section. From the Maxwell equations, using the corresponding boundary conditions at the interface, for the SPP guided mode, we find the eikonal as $\varphi = k_0 \int n(z)dz$, where $n(z)$ is the effective surface index of the plasmonic waveguide at a point z, which is determined by the equation

$$\frac{\varepsilon_m}{\kappa_m}\frac{I_1(k_0\kappa_m R)}{I_0(k_0\kappa_m R)} + \frac{\varepsilon_d}{\kappa_d}\frac{K_1(k_0\kappa_d R)}{K_0(k_0\kappa_d R)} = 0 \ , \qquad (64)$$

where I_p and K_p ($p = 0, 1$) are the modified Bessel functions; the complex decrements of the field in the metal and dielectric are: $\kappa_m = \sqrt{n^2 - \varepsilon_m}$ and $\kappa_d = \sqrt{n^2 - \varepsilon_d}$. This equation determines n as a function of the local wire radius R, which together with the grading dependence $R = R(z)$ defines the required effective index $n(z)$. Under the conventional plasmonic condition $\mathrm{Re}\varepsilon_m < -\varepsilon_d$,

Eq. (64) has nearly real solutions corresponding to the propagating SPP's. For a thick wire ($k_0 R \gg 1$), the solution is, understandably, the same as for the flat surface, $n = \sqrt{\varepsilon_m \varepsilon_d / (\varepsilon_m + \varepsilon_d)}$. For a thin, nanoscale-radius wire ($k_0 R \ll 1$) with logarithmic precision, we have

$$n(R) \approx \frac{1}{k_0 R} \sqrt{-\frac{2\varepsilon_d}{\varepsilon_m}} \left[\ln \sqrt{-\frac{4\varepsilon_m}{\varepsilon_d}} - \gamma \right]^{-1} , \qquad (65)$$

where $\gamma \approx 0.57721$ is the Euler constant. Note that at the tip $n \to \infty$, and SPP's do asymptotically stop, i.e., both the phase velocity $v_p = c/n$ and group velocity $v_g = c[d(n\omega)/d\omega]^{-1}$ tend to zero $\propto k_0 R$ for $k_0 R \to 0$. The point $R = 0$ (or $z = 0$) is an essential singularity. The time to reach this point $\propto \int n(R)dR \propto -\ln(k_0 R) \to \infty$ diverges logarithmically.

The eikonal parameter (also called WKB or adiabatic parameter) is defined as $\delta = \left| R' d(k_0 n)^{-1}/dR \right|$, where $R' = dR/dz$ is the wire grading. For the applicability of the eikonal (WKB) approximation, it necessary and sufficient that $\delta \ll 1$. At the nanoscale tip of the wire, which is the critical site for the adiabaticity (eikonal approximation applicability), from Eq. (65) we obtain

$$\delta \approx \left| R' \sqrt{-\frac{\varepsilon_m}{2\varepsilon_d}} \left[\ln \sqrt{-\frac{4\varepsilon_m}{\varepsilon_d}} - \gamma \right] \right| .$$

Thus, δ stays finite at the tip and can be made small enough by choosing sufficiently small grading R', so *the eikonal approximation is valid for the entire wire waveguide, including the stopping point at the tip.* This conclusion does not rely or significantly depend on $\mathrm{Im}\,\varepsilon_m$ (the optical losses in the system).

In our example, the tapered nanoplasmonic waveguide is a silver cone in vacuum with $R' = -0.02$; its angle of opening is 0.04 radian, as shown in Fig. 11(a). The vacuum reduced wavelength of the excitation radiation is $\lambdabar = 100$ nm, which corresponds to red light of $\lambda = 630$ nm. The SPPs are efficiently excited at the wide end of the waveguide nanowire by using, e.g., grating or Kretschmann[59,60] geometry and propagate to the tip as indicated. This propagation causes accumulation of the SPP energy at the tip and the corresponding increase of the local fields by more than three orders of magnitude. As shown in Fig. 11 (b), the intensity of the local optical field is sharply concentrated in 3D in a nanolayer at the surface of the metal, which is a signature of SPPs. In this figure, as everywhere in this Section, we show all lengths in units of $\lambdabar$, so the sizes range from the micro- to nanoscale. The hot spot of local fields is created in a nanosize region at the very tip. If it were not a plasmonic nanowire waveguide, but the conventional tapered optical fiber supporting guided photonic modes, than there would be a cut-off at some waveguide radius beyond which the propagation is not possible:[61] the wave is reflected back with only a short evanescent tail in the forward direction; no field enhancement would occur, and only an exponentially small part of the incident energy would reach the tip.

Mark I. Stockman

It was suggested earlier[62] that the propagation of SPPs toward the tip can produce energy concentration. It was also noted[63] that at the cut-off point, the guided photonic modes of an optical fiber could couple to the plasmonic modes of its metal coating causing further transfer of optical energy to the tip. However, no role of the adiabatic slowing-down and stopping of SPPs was previously elucidated. It is feasible that the observed[41] high efficiency of a metal tip on aperture probe is due to the proposed effect of the adiabatic accumulation.

The physical reason that the nanoplasmonic waveguide is an efficient energy concentrator can be inferred from Fig. 12(a). Both the phase and group velocity of SPPs asymptotically tend to zero toward the nanotip. Consequently, the SPPs are
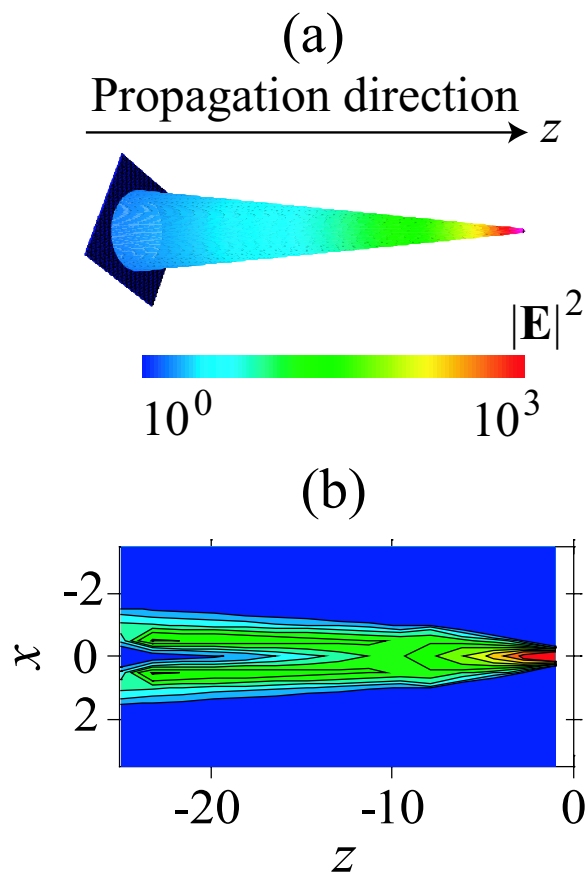

Fig. 11. (a) Geometry of the nanoplasmonic waveguide. The propagation direction of the SPP's is indicated by the arrow. Intensity $I(\mathbf{r}) = |\mathbf{E}(\mathbf{r})|^2$ of the local fields relative to the excitation field is shown by color. The scale of the intensities is indicated by the color bar in the center. (b) Local electric field intensity $I(\mathbf{r})$ is shown in the longitudinal cross section of the system. The coordinates are indicated in the units of the reduced radiation wavelength in vacuum, $\lambdabar = 100$ nm. The radius of the waveguide gradually decreases from 50 to 2 nm.

slowed down and adiabatically stopped at $z \to 0$, which leads to their accumulation at the tip. Correspondingly, in Fig. 12 (b) the local optical field is oscillating in space with progressively decreasing wavelength and its amplitude increasing by more than an order of magnitude. The highest enhancement is in fact limited only by the minimum tip size that can be considered on the basis of continuous electrodynamics. Importantly, being adiabatic to prevent the back reflection and 3D scattering, this process should be as rapid as possible to prevent losses in the metal.
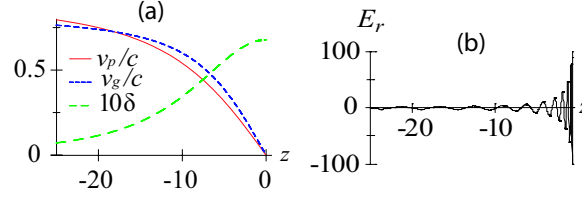

Fig. 12.   (a) Phase velocity v_p, group velocity v_g, and adiabatic parameter δ (scaled by a factor of 10) are shown as functions of the plasmonic waveguide radius. (b) Radial optical electric field at the surface of the metal nanowire waveguide in the units of the excitation field against the coordinate (in the propagation direction).

In Fig. 12 (a), along with the phase velocity v_p and group velocity v_g, we show also the adiabatic (WKB) parameter δ. It is of principal importance that this adiabatic parameter does stay finite and small, $\delta \leq 0.07$, throughout the entire system, ensuring the global applicability of the eikonal approximation, including the essentially singular point at $z = 0$.

The SPP electric fields are found from the Maxwell equations in eikonal (WKB) approximation in the form:

$$E_z(r, z) = \theta(R - r)I_0(k_0\kappa_m r) + \theta(r - R)BK_0(k_0\kappa_d r) ,$$
$$E_z(r, z) = \theta(R - r)i\frac{n}{\kappa_m}I_1(k_0\kappa_m r)$$
$$+ \theta(r - R)i\frac{n}{\kappa_d}BK_1(k_0\kappa_d r) , \tag{66}$$

where $B = I_0(k_0\kappa_m R)/K_0(k_0\kappa_m R)$, and $\theta(\dots)$ denotes the Heaviside θ-function. To determine the pre-exponential $A(z)$ in Eq. (63), we use the energy flux conservation in terms of the Pointing vector integrated over the normal (xy) plane, obtaining

$$A \propto \text{Re}\left[\frac{n^*\varepsilon_m^*}{|\kappa_m|^2}|K_0(k_0\kappa_d R)|^2\int_0^R |I_1(k_0\kappa_m r)|^2 rdr\right.$$
$$\left. + \frac{n^*\varepsilon_d^*}{|\kappa_d|^2}|I_0(k_0\kappa_m R)|^2\int_R^\infty |K_1(k_0\kappa_d r)|^2 rdr\right]^{-\frac{1}{2}} , \tag{67}$$

where all the spatially-varying quantities, n, κ_m, and κ_d, are functions of local radius R of the wire, as originally given by Eq. (64). The required dependence

Mark I. Stockman

$A = A(z)$ is obtained by substituting the grading relation $R = R(z)$. We indicate only the proportionality of A: the total scale of A is undetermined by the equations and is defined by the total power of the propagating SPP wave. This completes the eikonal (WKB) solution.

The intensity of the optical electric fields has already been discussed in conjunction with Fig. 11 where they are shown on the logarithmic scale. For this example and below, we set the minimum radius of the wire to be $R_{min} = 0.02\lambda = 2$ nm to avoid effects of the spatial dispersion of the dielectric response that are important at shorter distances, cf. Refs.,[64,65] and the maximum radius (at $z = -25\lambda = -2.5$ μ) to be $R_{max} = 0.5\lambda = 50$ nm.
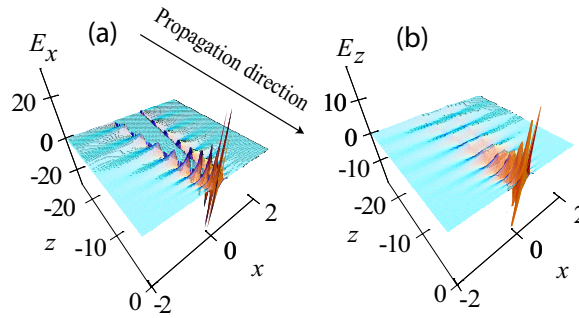

Fig. 13.   Snapshot of instantaneous fields (at some arbitrary moment $t = 0$): Normal component E_x (a) and longitudinal component E_z (b) of the local optical electric field are shown in the longitudinal cross section (xz) plane of the system. The fields are in the units of the far-zone (excitation) field.

In Fig. 13, we display the amplitudes of the local optical fields in the cross section of the system for the normal and longitudinal (with respect to the axis) components of the optical electric field. In Fig. 13, far from the tip of the nanoplasmonic waveguide, the optical electric field is mostly transverse, extending in vacuum to distances $\sim \lambda$ where most of the SPP field is propagating. The longitudinal field in the metal is very small, proportional to a factor of $|\varepsilon_d/\varepsilon_m| \ll 1$, as should be from the boundary conditions. Therefore, the guide itself is clearly seen in panel (a) as the acute triangular region of low fields. As SPPs move toward the tip, the SPP fields start to localize at the metal surface, and simultaneously, their wavelength is progressively reducing and amplitude growing. Because the very tip is not included, the singularity point of the fields does not show in these figures. Even with this truncation, the field magnitudes grow significantly at small $|z|$. The transverse x component grows by an order of magnitude as the SPPs approach the tip of the guide, while the longitudinal z component, which is very small far from the tip, grows relatively much stronger. Close to the tip, both these components are on the same order of magnitude, as is expected for the localized excitations. This growth in magnitude is concurrent with the energy localization in 3D and the significant reduction of the wavelength, which are due to the dramatic slowing down of the

SPPs. Note the SPPs in Fig. 13 are not standing but running waves; the fields shown represent an instantaneous snapshot of these waves.
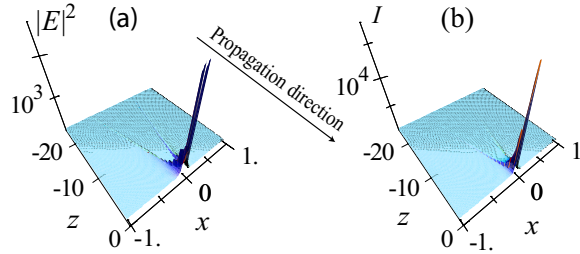

Fig. 14.   Mean (time averaged) intensity $I(\mathbf{r})$ (a) and the energy density $W(\mathbf{r})$ (b) of the local optical electric field in the xy plane of the system. The magnitudes are relative to those of the excitation wave.

In Fig. 14, we show the spatial behavior of relative intensity $I(\mathbf{r})$ and energy density[48] $W(\mathbf{r}) = \{d[\omega\varepsilon(\mathbf{r},\omega)]/d\omega\}\,|\mathbf{E}|^2$ of the local optical electric field. The intensity grows by more than three and energy density by four orders of magnitude at the tip. If these fields were used to induce SERS, it would be enhanced by seven to eight orders of magnitude. The further enhancement of SERS by many orders of magnitude can be achieved by positioning a resonant nanolens[66] at the tip of the nanoplasmonic waveguide. Note that $|\mathbf{E}|^2$ is concentrated at the outer surface of the metal nanowire, with the exponential decay far from this surface. In contrast, a metal nanoparticle excited by an external field would produce dipolar local fields where $|\mathbf{E}|^2 \propto r^{-6}$. At the same time, $I(\mathbf{r})$ is significantly larger and *localized inside the metal plasmonic waveguide where most of the SPP energy is propagating* due to the large value of $d[\omega\varepsilon(\mathbf{r},\omega)]/d\omega$ for metals.

At the foundation of the above-described high-efficiency coupling of the far-field radiation to the near-field is the adiabatic slow-down of the running, propagating SPPs and their gradual conversion into standing, SP-like modes. The 3D energy concentration occurs at the tip of a smoothly tapered metal nanoplasmonic waveguide. This causes the local field increase by three orders of magnitude in intensity and four orders in energy density. The stopping of SPPs is asymptotic, i.e., they need logarithmically divergent time to reach the tip, which mathematically is the point of an essential singularity. Similar phenomena are likely to exist for a hollow tapered waveguides, in particular subwavelength holes. The rapid adiabatic nanofocusing promises to find various applications in nanooptics and nanotechnology where greatly enhanced local optical fields are required, in particular, for probing, spectroscopy, detection, and modification on the nanoscale in physics, chemistry, biology, electrical engineering, etc.

2.7.1. *Experimental Observations of Adiabatic SPP Concentration*

Following the publication of the original theoretical proposal,[10,44] there has been several experimental confirmations of this concept. The adiabatic concentration of SPPs manifested by enhanced local optical fields around a tip of the nanoplasmonic tapered planar wedge have been recently observed.[67,68] This energy concentration is accompanied by greatly enhanced nonlinear- optical effects. A very original method using upconverted far-field fluorescence of rear-earth ions have been used in these studies to visualize the *near-field* optical energy. The principal possibility of such a method is based on the fact the upconverted wavelength is much shorter than the fundamental wavelength in vacuum; thus far-field observation of the upconverted radiation allows one to see the near fields of the SPPs at the fundamental frequency. The observed phenomena are in a good qualitative agreement with the above theory. However, he quantitative comparison is difficult because of the planar geometry (metal wedge on a substrate) in the experiment and the cylindrical one in the theory.

An independent confirmation has been obtained in an experiment using a free-standing silver cone.[69] In this experiment, the SPPs are excited using a grating coupler cut into a side of the cylinder. A strongly enhanced emission has been observed in the far-field using a confocal optical microscope from the tip of the cone. It is likely that this emission is caused by outcoupling of light from the cone due to the some roughness of the silver surface. Very promising is combination of the adiabatic SPP concentration with the electron emission, which, similar to Ref. 70 will allow for the creation of nanoscale sources electron pulses. In combination with the ideas of the coherent control,[15,31,37] it is possible to make this nanoscale electron source also ultrafast, producing femtosecond electron pulses. Such sources can have a wide range of applications in science and engineering.

3. Nanoplasmonic Active Phased Array (NAPAR)

3.1. *Introduction to Spatio-Temporal Coherent Control*

Two novel areas of optics have recently attracted a great deal of attention: nanooptics and ultrafast optics. One of the most rapidly developing directions in ultrafast optics is quantum control, in which coherent superpositions of quantum states are created by excitation radiation to control the quantum dynamics and outcomes.[22,25,71,72] Of special interest are coherently controlled ultrafast phenomena on the nanoscale where the phase of the excitation waveform along with its polarization provides a functional degree of freedom to control the nanoscale distribution of energy.[15,31–34,36,73] Spatiotemporal pulse shaping permits one to generate dynamically predefined waveforms modulated both in frequency and in space to focus ultrafast pulses in the required microscopic spatial and femtosecond temporal domains.[74,75]

In this Section, we theoretically describe a method of full coherent control on the nanoscale proposed in Ref. 37. In this method, a spatio-temporally modulated waveform is launched in a graded nanostructured system, specifically a wedge. Its propagation from the thick (macroscopic) to the thin (nanoscopic) edge of the wedge and the concurrent adiabatic concentration provide a possibility to focus the optical energy in *nanoscale* spatial and femtosecond temporal regions. This method unifies three approaches that individually have been developed and experimentally tested. The coupling of the external radiation to the surface plasmon polaritons (SPPs) propagating along the wedge occurs through an array of nanoobjects (nanoparticles or nanoholes) that is situated at the thick edge of the wedge. The phases of the SPPs emitted (scattered) by individual nanoobjects are determined by a spatio-temporal modulator. The nanofocusing of the SPPs occurs due to their propagation toward the nanofocus and the concurrent adiabatic concentration.

The coupling of the external radiation to SPPs and their nanofocusing have been observed – see, e.g., Refs. 76,77. The second component of our approach, the spatio-temporal coherent control of such nanofocusing has been developed.[74,75] The third component, the adiabatic concentration of SPPs also has been recently observed.[67,69] The idea of adiabatic concentration is described above in Sec. 2. It is based on adiabatic following by a propagating SPP wave of a graded plasmonic waveguide, where the phase and group velocities decrease while the propagating SPP wave is adiabatically transformed into a standing surface plasmon (SP) mode. A new quality that is present in our approach is a possibility to arbitrary move the nanofocus along the nanoedge of the wedge. Moreover, it is possible to super-impose any number of such nanofoci simultaneously and, consequently, create any distribution of the nanolocalized fields at the thin edge of the wedge.

The idea of the spatio-temporal coherent control is analogous to that of the synthetic aperture radar (SAR) and conceptually similar active phased array radar (APAR), or active electronically scanned array (AESA) radar widely used in military and civilian radar systems. This idea can be introduced using a schematic shown in Fig. 15. An APAR consists of active oscillators that act as dipole antennas (shown by bold short vertical segments). Each of these antennas generates a pulse of radiation whose phase is controlled elctronically. If the phases are equal, as in Fig. 15(a), the beam produced by the interference of the waves emitted by each of the antennas is straight with the wavefront parallel to the array base. If there is a linear phase shift, as in panel (b), the beam is steered toward the emitters with retarded phases. For a parabolic-type modulation of the phases along the base line with a maximum phase delay in the center, a focused beam is formed as in panel (c). And finally, a linear combination of the linear and focusing phase shifts leads to the simultaneous steering and focusing as shown in Fig. 15(d). Due to the superposition principle, any superposition of the beams can be created by the correspondingly superimposing the phase modulations, provided that the number of the active antennas is large enough.

Mark I. Stockman

The idea of this full coherent control is APAR transferred to the nanoplasmon-ics, which can be called Nanoplasmonic Active Phased Array "Radar" (NAPAR). This can be complemented with the adiabatic nanofocusing to further increase the concentration of the optical energy. To introduce it consider a schematic in Fig. 16. As shown, a nanoplasmonic wedge contains a line of nano-size scatterers (shown as nanospheres) located at the thick edge and parallel to it, i.e. in the x direction in Fig. 16 (b). These scatters play the role if the emitting dipoles in NAPAR and can be either nanoparticles of various shapes and compositions, nanoholes, or elements of the surface roughness.

Consider first monochromatic light irradiating these nanoparticles or nanoholes that scatter and couple it into SPP wavelets, shown as red arc segments in Fig. 16. Every such a scatterer emits SPPs in all directions; there is, of course, no favored directionality of the scattering. However, we assume that the excitation radiation and, correspondingly, the scattered wavelets of the SPP are coherent, and their phases smoothly vary in space along the thick edge, i.e., in the x direction. The SPP wavelets emitted by different scatterers will interfere, which in accord with the Huygens-Fresnel principle leads to formation of a smooth wavefront of the SPP wave at some distance from the scatterers in the far SPP field. This distance, of course, must be much greater than the spacing of the scatterers.

Such wavefronts are shown in Fig. 16 (b) with concave black curves. The energy of the SPP is transferred along the rays, which are lines normal to the wavefronts, shown by the colored lines. By the appropriate spatial phase modulation of the excitation radiation along the line of scatterers over distances of many SPP wave-
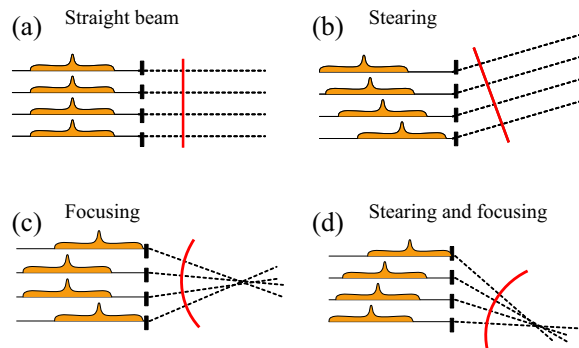

Fig. 15.   Schematic of the Active Phased Array Radar (APAR). The short solid elements indicated the active dipoles (oscillators) of the antenna array. The dashed horizontal lines show the ray propagation in the far field of the array. The solid vertical red line shows the wavefront of the radar pulse. The individual pulses fed to (for a passive array) generated by the array oscillators (for an active array) are indicated by the waveforms shown above the corresponding rays. (a): Case of the straight beam (wavefront parallel to the array base) where there is no phase delay between the oscillators. (b) Beam steering: There is a phase delay between the oscillator pulses increasing linearly from bottom to the top. (c) Beam focusing: the phase delays are minimum at the center and maximum at the edges to form a spherical wavefront. (d) Beam staring and focusing: the phase delays are a combination of a linear shift and parabolic modulation.

lengths, these wavefronts can be formed in such a way that the rays intersect at a given point, forming a nanofocus at the thin (sharp) edge of the wedge, as shown schematically in Fig. 16 (b). Diffraction of the SPP waves will lead to a finite size of this focal spot that we will estimate later in this Section.

By changing the spatial phase profile of the excitation radiation, this focal spot can be arbitrarily moved along the thin edge. This focusing and adiabatic concentration, as the SPPs slow down approaching the sharp edge, will lead to the enhancement of the intensity of the optical fields in the focal region. This dynamically-controlled concentration of energy is a plasmonic counterpart of a large phased antenna array (also known as an aperture synthesis antenna or beamformer), widely used in radar technology and radio astronomy.[78] Now we can consider excitation by spatiotemporally shaped ultrashort pulses.[74,75] The field produced by them is a coherent superposition of waves with different frequencies whose amplitudes and phases can arbitrarily vary in space and with frequency. This modulation can be chosen so that all the frequency components converge at the same focal spot at the same time forming an ultrashort pulse of the nanolocalized optical fields.

Turning to the theory, consider a nanofilm of metal in the xy plane whose thickness d in the z direction is adiabatically changing with the coordinate-vector $\boldsymbol{\rho} = (x, y)$ in the plane of the nanofilm. Let $\varepsilon_m = \varepsilon_m(\omega)$ be the dielectric permittivity of this metal nanofilm, and ε_d be the permittivity of the embedding dielectric. As we discussed in Sec. 2.4, due to the symmetry of the system, there are odd and even (in the normal electric field) SPPs. It is the odd SPP that is a slow-propagating, controllable mode. The dispersion relation for this mode defining its effective index $n(\boldsymbol{\rho})$ is given by Eq. 32, which can be explicitly rewritten as

$$\tanh\left(\frac{1}{2}k_0 d(\boldsymbol{\rho})\sqrt{n(\boldsymbol{\rho})^2 - \varepsilon_m}\right) = -\frac{\varepsilon_d\sqrt{n(\boldsymbol{\rho})^2 - \varepsilon_m}}{\varepsilon_m\sqrt{n(\boldsymbol{\rho})^2 - \varepsilon_d}} \ , \tag{68}$$

where $k_0 = \omega/c$ is the radiation wave vector in vacuum.

Let $\boldsymbol{\tau}$ be a unit tangential vector to the SPP trajectory (ray). It obeys an equation of ray optics[48] $n\,(d\boldsymbol{\tau}/dl) = \partial n/\partial\boldsymbol{\rho} - \boldsymbol{\tau}\,(\boldsymbol{\tau}\partial n/\partial\boldsymbol{\rho})$, where l is the length along the ray.

Now let us consider a nanofilm shaped as a nanowedge as in Fig. 16(b), see also theory of Sec. 2.6. In such a case, $n = n(y)$, and these trajectory equations simplify as $n\,(d\tau_y/dl) = \tau_x^2\,(dn/dy)$, $n\,(d\tau_x/dl) = -\tau_x\tau_y\,(dn/dy)$. From these, it follows that $n_x \equiv \tau_x n = \text{const}$. The SPP wave vector, related to its momentum, is $\mathbf{k}(\boldsymbol{\rho}) = k_0 n(\boldsymbol{\rho})\boldsymbol{\tau}$; this is the conservation of k_x (the transverse momentum). This allows one to obtain a closed solution for the ray. The tangent equation for the ray is $dx/dy = \tau_x/\tau_y$, where $\tau_y = \sqrt{1 - n_x^2/n^2}$. From this, we get an explicit SPP ray equation as

$$x - x_0 = \int_{y_0}^{y}\left(\frac{n(y')^2}{n_x^2} - 1\right)^{-1/2} dy' \ , \tag{69}$$

where $\boldsymbol{\rho}_0 = (x_0, y_0)$ is the focal point where rays with any n_x converge. To find the trajectories, as $n(y)$ we use the real part of effective index (68), as WKB suggests.

When the local thickness of the wedge is subwavelength ($k_0 d \ll 1$), the form of these trajectories can be found analytically. Under these conditions, dispersion relation (68) has an asymptotic solution

$$n = \frac{n_a}{k_0 d} \ , \quad n_a = \ln \frac{\varepsilon_m - \varepsilon_d}{\varepsilon_m + \varepsilon_d} \ . \tag{70}$$

Substituting this into Eq. (69), we obtain an explicit SPP ray equation $\left(x - x_0 - \sqrt{\bar{n}_a^2 / n_x^2 - y_0^2} \right)^2 + y^2 = \bar{n}_a^2 / n_x^2$, where $\bar{n}_a = n_a/(k_0 \tan \theta)$, and $\tan \theta$ is the slope of the wedge. Thus, each SPP ray is a segment of a circle whose center is at a point given by $x = x_0 + \sqrt{(\bar{n}_a/n_x)^2 - y_0^2}$ and $y = 0$. This analytical result is in agreement with Fig. 16 (b). If the nanofocus is at the sharp edge, i.e., $y_0 = 0$, then these circles do not intersect but touch and are tangent to each other at the nanofocus point.

As an example we consider a silver[51] nanowedge illustrated in Fig. 16 (b) whose maximum thickness is $d_m = 30$ nm, the minimum thickness is $d_f = 4$ nm, and whose length (in the y direction) is $L = 5$ μm. Trajectories calculated from Eq. (69) for $\hbar\omega = 2.5$ eV are shown by lines (color used only to guide eye); the nanofocus is indicated by a bold red dot. The different trajectories correspond to different values of n_x in the range $0 \le n_x \le n(L)$. In contrast to focusing by a conventional lens, the SPP rays are progressively bent toward the wedge slope direction.

The eikonal is found as an integral along the ray $\Phi(\boldsymbol{\rho}) = \int_{\boldsymbol{\rho}_0}^{\boldsymbol{\rho}} \mathbf{n}(\boldsymbol{\rho}) d\boldsymbol{\rho}$. Consider rays emitted from the nanofocus [Fig. 16 (b)]. Computed from this equation, the phases of the SPPs at the thick edge of the wedge (for $y = L$) are shown in Fig. 17 (a) as functions of the coordinate x along the thick edge. The colors of the rays correspond to the visual perception of the ray frequencies. The gained phase dramatically increases toward the blue spectral region, exhibiting a strong dispersion. The extinction for most of the frequencies except for the blue edge, displayed in Fig. 17 (b), is not high.

Now consider the evolution of the field intensity along a SPP ray. For certainty, let SPPs propagate along the corresponding rays from the thick edge of the wedge toward the nanofocus as shown in Fig. 16 (b). In the process of such propagation, there will be concentration of the SPP energy in all three directions (3d nanofocusing). This phenomenon differs dramatically from what occurs in conventional photonic ray optics.

To describe this nanofocusing, it is convenient to introduce an orthogonal system of ray coordinates whose unit vectors are $\boldsymbol{\tau}$ (along the ray), $\boldsymbol{\eta} = (-\tau_y, \tau_x)$ (at the surface normal to the ray), and $\mathbf{e}_z$ (normal to the surface). The concentration along the ray (in the $\boldsymbol{\tau}$ direction) occurs because the group velocity $v_g = [\partial(k_0 n)/\partial\omega]^{-1}$ of SPP asymptotically tends to zero (for the antisymmetric mode) for $k_0 d \to 0$ as $v_g = v_{0g} d$ where $v_{0g} = \text{const.}$[10] This contributes a factor $A_\parallel = 1/\sqrt{v_g(d)}$ to the amplitude of an SPP wave.

The compression of a SPP wave in the $\mathbf{e}_z$ (vertical) direction is given by a factor of $A_z = \left(\int_{-\infty}^{\infty} W \mathrm{d}z \right)^{-1/2}$, where W is the energy density of the mode. Substituting a standard expression[48] for W, one obtains explicitly

$$A_z = \left(\frac{1}{8\pi} \exp\left(\mathrm{Re}\,\kappa_d d\right) \left\{ \vphantom{\frac{\sinh}{\sinh}} \right.\right.$$

$$\frac{\sinh\left(\mathrm{Re}\,\kappa_m d\right)}{\mathrm{Re}\,\kappa_m \left|\sinh\left(\kappa_m d/2\right)\right|^2} \left[1 + \frac{d(\omega \mathrm{Re}\,\varepsilon_m)}{d\omega} \frac{|n|^2 + |\kappa_m|^2}{|\varepsilon_m|^2} \right] -$$

$$\frac{\sin\left(\mathrm{Im}\,\kappa_m d\right)}{\mathrm{Im}\,\kappa_m \left|\sinh\left(\kappa_m d/2\right)\right|^2} \left[1 + \frac{d(\omega \mathrm{Re}\,\varepsilon_m)}{d\omega} \frac{|n|^2 - |\kappa_m|^2}{|\varepsilon_m|^2} \right] +$$

$$\left.\left. \frac{2}{\mathrm{Re}\,\kappa_d} \left[1 + \frac{|n|^2 + |\kappa_d|^2}{\varepsilon_d} \right] \right\} \right)^{-1/2}, \tag{71}$$

where $\kappa_m = k_0 \sqrt{n - \varepsilon_m}$ and $\kappa_d = k_0 \sqrt{n - \varepsilon_d}$. Note that the intensity distribution in Fig. 16 (a) is $I \propto \left(A_\parallel A_z \right)^{-2}$.

To obtain the compression factor $A_\perp$ for the $\boldsymbol{\eta}$ direction), we consider conservation of energy along the beam of rays corresponding to slightly different values of n_x. Dividing this constant energy flux by the thickness of this beam in the $\boldsymbol{\eta}$ direction, we arrive at

$$A_\perp = \left\{ \left(1 - \frac{n_x^2}{n^2} \right)^{1/2} \int_{y_0}^{y} \frac{1}{n(y')} \left[1 - \frac{n_x^2}{n(y')^2} \right]^{-3/2} \mathrm{d}y' \right\}^{-1/2}. \tag{72}$$

The ray amplitude thus contains the total factor which describes the 3d adiabatic compression: $A = A_\parallel A_\perp A_z$.

Now consider the problem of coherent control. The goal is to excite a spatiotemporal waveform at the thick edge of the wedge in such a way that the propagating SPP rays converge at an arbitrary nanofocus at the sharp edge where an ultrashort pulse is formed. To solve this problem, we use the idea of back-propagation or time-reversal.[79–81] We generate rays at the nanofocus as an ultrashort pulse containing just several oscillations of the optical field. Propagating these rays, we find amplitudes and phases of the fields at the thick edge at each frequency as given by the eikonal $\Phi(\boldsymbol{\rho})$. Then we complex conjugate the amplitudes of frequency components, which corresponds to the time reversal. We also multiply these amplitudes by $\exp(2\mathrm{Im}\,\Phi)$ which pre-compensates for the losses. This provides the required phase and amplitude modulation at the thick edge of the wedge.

We show an example of such calculations in Fig. 18. Panel (a) displays the trajectories of SPPs calculated according to Eq. (69). The trajectories for different frequencies are displayed by colors corresponding to their visual perception. There is a very significant spectral dispersion: trajectories with higher frequencies are much more curved. The spatial-frequency modulation that we have found succeeds in bringing all these rays (with different frequencies and emitted at different

x points) to the same nanofocus at the sharp edge.

The required waveforms at different x points of the thick edge of the wedge are shown in Fig. 18 (b)-(d) where the corresponding longitudinal electric fields are shown. The waves emitted at large x, i.e., at points more distant from the nanofocus, should be emitted significantly earlier to pre-compensate for the longer propagation times. They should also have different amplitudes due to the differences in A. Finally, there is clearly a negative chirp (gradual decrease of frequency with time). This is due to the fact that the higher frequency components propagate more slowly and therefore must be emitted earlier to form a coherent ultrashort pulse at the nanofocus.

In Fig. 18 (e) we display together all three of the representative waveforms at the thick edge to demonstrate their relative amplitudes and positions in time. The pulse at the extreme point in x (shown by blue) has the longest way to propagate and therefore is the most advanced in time. The pulse in the middle point (shown by green) is intermediate, and the pulse at the center ($x = 0$, shown by red) is last. One can notice also a counterintuitive feature: the waves propagating over longer trajectories are smaller in amplitude though one may expect the opposite to compensate for the larger losses. The explanation is that the losses are actually insignificant for the frequencies present in these waveforms, and the magnitudes are determined by adiabatic concentration factor A.

Figure 18 (e) also shows the resulting ultrashort pulse in the nanofocus. This is a transform-limited, Gaussian pulse. The propagation along the rays completely compensates the initial phase and amplitude modulation, exactly as intended. As a result, the corresponding electric field of the waveform is increased by a factor of 100. Taking the other component of the electric field and the magnetic field into account, the corresponding increase of the energy density is by a factor $\sim 10^4$ with respect to that of the SPPs at the thick edge.

Consider the efficiency of the energy transfer to the nanoscale. This is primarily determined by the cross section σ_{SPP} for scattering of photons into SPPs. For instance, for a metal sphere of radius R at the surface of the wedge, one can obtain an estimate $\sigma_{SPP} \sim R^6/(d_m^3 \lambda)$, where λ is the reduced photon wavelength. Setting $R \sim d_m$, we estimate $\sigma_{SPP} \sim 3 \text{ nm}^2$. Assuming optical focusing into a spot of ~ 300 nm radius, this yields the energy efficiency of conversion to the nanoscale of $\sim 10^{-3}$. Taking into account the adiabatic concentration of energy by a factor of 10^4, the optical field intensity at the nanofocus is enhanced by one order of magnitude with respect to that of the incoming optical wave.

The criterion of applicability of the WKB approximation is $\partial k^{-1}/\partial y \ll 1$. Substituting $k = k_0 n$ and Eq. (70), we obtain a condition $d_m/(n_a L) << 1$. This condition is satisfied everywhere including the nanofocus since $n_a \sim 1$ and $d_m \ll L$ for adiabatic grading. The minimum possible size of the wavepacket at the nanofocus in the direction of propagation, Δx, is limited by the local SPP wavelength: $\Delta x \sim 2\pi/k \approx 2\pi d_f/n_a$. The minimum transverse size a (waist) of the SPP

beam at the nanofocus can be calculated as the radius of the first Fresnel zone: $a = \pi/k_x \geq \pi/(k_0 n_x)$. Because n_x is constant along a trajectory, one can substitute its value at the thick edge (the launch site), where from Eq. (70) we obtain $n_x \approx n = n_a/d_m$. This results in $a \approx \pi d_m/n_a$; thus a is on order of the maximum thickness of the wedge, which is assumed also to be on the nanoscale.

To briefly conclude, we have theoretically described an approach to full coherent control of spatiotemporal energy localization on the nanoscale. From the point of view of electromagnetics this concept is a nanoplasmonic counterpart of the active phased array radar (APAR) and can be called NAPAR. As we described, in NAPAR from the thick edge of a plasmonic metal nanowedge, SPPs are launched, whose phases and amplitudes are independently modulated for each constituent frequency of the spectrum and at each spatial point of the excitation. This pre-modulates the departing SPP wave packets in such a way that they reach the required point at the sharp edge of the nanowedge in phase, with equal amplitudes forming a nanofocus where an ultrashort pulse with required temporal shape is generated. Of course, a similar control can be achieved on a nanoplasmonic slab of a constant thickness, but then the benefit of the adiabatic nanofocusing would be lost. The system described (NAPAR) constitutes a "nanoplasmonic portal" connecting the incident light field, whose features are shaped on the microscale, with the required point or features at the nanoscale.

4. Acknowledgments

References

1. L. Novotny and B. Hecht, *Principles of Nano-Optics*. (Cambridge University Press, Cambridge, New York, 2006).
2. Near-field optics and surface plasmon polaritons. In ed. S. Kawata, *Topics in Applied Physics*, vol. 81. Springer Verlag, Berlin, New York, (2001).
3. M. I. Stockman, S. V. Faleev, and D. J. Bergman, Localization versus delocalization of surface plasmons in nanosystems: Can one state have both characteristics?, *Phys. Rev. Lett.* **87**, 167401–1–4, (2001).
4. M. I. Stockman, M. F. Kling, U. Kleineberg, and F. Krausz, Attosecond nanoplasmonic field microscope, *Nature Photonics.* **1**, 539–544, (2007).
5. T. Klar, M. Perner, S. Grosse, G. von Plessen, W. Spirkl, and J. Feldman, Surface-plasmon resonances in single metallic nanoparticles, *Phys. Rev. Lett.* **80**, 4249–4252, (1998).
6. J. Lehmann, M. Merschdorf, W. Pfeiffer, A. Thon, S. Voll, and G. Gerber, Surface

Mark I. Stockman

plasmon dynamics in silver nanoparticles studied by femtosecond time-resolved photoemission, *Phys. Rev. Lett.* **85**, 2921–2924, (2000).

7. J. Bosbach, C. Hendrich, F. Stietz, T. Vartanyan, and F. Trager, Ultrafast dephasing of surface plasmon excitation in silver nanoparticles: Influence of particle size, shape, and chemical surrounding, *Phys. Rev. Lett.* **89**, 257404–1–4, (2002).

8. C. Hendrich, J. Bosbach, F. Stietz, F. Hubenthal, T. Vartanyan, and F. Trager, Chemical interface damping of surface plasmon excitation in metal nanoparticles: A study by persistent spectral hole burning, *Appl. Phys. B.* **76**, 869–875, (2003).

9. T. Zentgraf, A. Christ, J. Kuhl, and H. Giessen, Tailoring the ultrafast dephasing of quasiparticles in metallic photonic crystals, *Phys. Rev. Lett.* **93**, 243901–1–4, (2004).

10. M. I. Stockman, Nanofocusing of optical energy in tapered plasmonic waveguides, *Phys. Rev. Lett.* **93**, 137404–1–4, (2004).

11. A. Ono, J. Kato, and S. Kawata, Subwavelength optical imaging through a metallic nanorod array, *Phys. Rev. Lett.* **95**, 267407–1–4, (2005).

12. G. Shvets, S. Trendafilov, J. B. Pendry, and A. Sarychev, Guiding, focusing, and sensing on the subwavelength scale using metallic wire arrays, *Phys. Rev. Lett.* **99**, 053903–1–4, (2007).

13. J. B. Pendry, Perfect cylindrical lenses, *Opt. Expr.* **11**, 755–760, (2003).

14. Z. Liu, H. Lee, Y. Xiong, C. Sun, and X. Zhang, Far-field optical hyperlens magnifying sub-diffraction-limited objects, *Science.* **315**, 1686–1686, (2007).

15. M. I. Stockman, S. V. Faleev, and D. J. Bergman, Coherent control of femtosecond energy localization in nanosystems, *Phys. Rev. Lett.* **88**, 067402–1–4, (2002).

16. D. J. Tannor and S. A. Rice, Control of selectivity of chemical reaction via control of wave packet evolution, *J. Chem. Phys.* **83**, 5013–5018, (1985).

17. In eds. P. Brumer and M. Shapiro, *Principles of the Quantum Control of Molecular Processes.* Wiley, New York, (2003).

18. R. S. Judson and H. Rabitz, Teaching lasers to control molecules, *Phys. Rev. Lett.* **68**, 1500, (1992).

19. G. Kurizki, M. Shapiro, and P. Brumer, Phase-coherent control of photocurrent directionality in semiconductors, *Phys. Rev. B.* **39**, 3435–3437, (1989).

20. T. C. Weinacht, J. Ahn, and P. H. Bucksbaum, Controlling the shape of a quantum wavefunction, *Nature.* **397**, 233–235, (1999).

21. P. Brumer and M. Shapiro, Laser control of molecular processes, *Ann. Rev. Phys. Chem.* **43**, 257–282, (1992).

22. H. Rabitz, R. de Vivie-Riedle, M. Motzkus, and K. Kompa, Chemistry - whither the future of controlling quantum phenomena?, *Science.* **288**, 824–828, (2000).

23. J. M. Geremia and H. Rabitz, Optimal identification of hamiltonian information by closed-loop laser control of quantum systems, *Phys. Rev. Lett.* **89**, 263902–1–4, (2002).

24. N. A. Nguyen, B. K. Dey, M. Shapiro, and P. Brumer, Coherent control in nanolithography: Rydberg atoms, *J. Phys. Chem. A.* **108**, 7878–7888, (2004).

25. M. Shapiro and P. Brumer, Quantum control of bound and continuum state dynamics, *Physics Reports.* **425**, 195–264, (2006).

26. A. Assion, T. Baumert, M. Bergt, T. Brixner, B. Kiefer, V. Seyfried, M. Strehle, and G. Gerber, Control of chemical reactions by feedback-optimized phase-shaped femtosecond laser pulses, *Science.* **282**, 919–922, (1998).

27. R. Bartels, S. Backus, E. Zeek, L. Misoguti, G. Vdovin, I. P. Christov, M. M. Murnane, and H. C. Kapteyn, Shaped-pulse optimization of coherent emission of high-harmonic soft x-rays, *Nature.* **406**, 164–166, (2000).

28. N. Dudovich, D. Oron, and Y. Silberberg, Single-pulse coherently controlled nonlinear raman spectroscopy and microscopy, *Nature.* **418**, 512–514, (2002).

29. T. Brixner, G. Krampert, T. Pfeifer, R. Selle, G. Gerber, M. Wollenhaupt, O. Graefe, C. Horn, D. Liese, and T. Baumert, Quantum control by ultrafast polarization shaping, *Phys. Rev. Lett.* **92**, 208301–1–4, (2004).

30. M. I. Stockman, D. J. Bergman, and T. Kobayashi, Coherent control of nanoscale localization of ultrafast optical excitation in nanosystems, *Phys. Rev. B.* **69**, 054202–1–10, (2004).

31. M. I. Stockman and P. Hewageegana, Nanolocalized nonlinear electron photoemission under coherent control, *Nano Lett.* **5**, 2325–2329, (2005).

32. M. Sukharev and T. Seideman, Phase and polarization control as a route to plasmonic nanodevices, *Nano Lett.* **6**, 715–719, (2006).

33. A. Kubo, K. Onda, H. Petek, Z. Sun, Y. S. Jung, and H. K. Kim, Femtosecond imaging of surface plasmon dynamics in a nanostructured silver film, *Nano Lett.* **5**, 1123–1127, (2005).

34. M. Aeschlimann, M. Bauer, D. Bayer, T. Brixner, F. J. G. d. Abajo, W. Pfeiffer, M. Rohmer, C. Spindler, and F. Steeb, Adaptive subwavelength control of nano-optical fields, *Nature.* **446**, 301–304, (2007).

35. M. Bauer, C. Wiemann, J. Lange, D. Bayer, M. Rohmer, and M. Aeschlimann, Phase propagation of localized surface plasmons probed by time-resolved photoemission electron microscopy, *Appl. Phys. A.* **88**, 473–480, (2007).

36. M. Sukharev and T. Seideman, Coherent control of light propagation via nanoparticle arrays, *J. Phys. B: At. Mol. Opt. Phys.* pp. S283–S298, (2007).

37. M. Durach, A. Rusina, K. Nelson, and M. I. Stockman, Toward full spatio-temporal control on the nanoscale, *Nano Lett.* **7**, 3145–3149, (2007).

38. A. A. Mikhailovsky, M. A. Petruska, K. Li, M. I. Stockman, and V. I. Klimov, Phase-sensitive spectroscopy of surface plasmons in individual metal nanostructures, *Phys. Rev. B.* **69**, 085401–1–6, (2004).

39. A. A. Mikhailovsky, M. A. Petruska, M. I. Stockman, and V. I. Klimov, Broadband near-field interference spectroscopy of metal nanoparticles using a femtosecond white-light continuum, *Optics Lett.* **28**, 1686–1688, (2003).

40. T. Kawazoe, T. Shimizu, and M. Ohtsu, Second-harmonic generation in a near-field optical-fiber probe, *Opt. Lett.* **26**, 1687–1689, (2001).

41. H. G. Frey, F. Keilmann, A. Kriele, and R. Guckenberger, Enhancing the resolution of scanning near-field optical microscopy by a metal tip grown on an aperture probe, *Appl. Phys. Lett.* **81**, 5030–5032, (2002).

42. F. Keilmann, Scattering-type near-field optical microscopy, *J. Electron. Microsc.* **53**, 187–192, (2004).

43. F. Keilmann and R. Hillenbrand, Near-field microscopy by elastic light scattering from a tip, *Philos. Trans. Roy. Soc. A.* **362**, 787–805, (2004).

44. M. I. Stockman. Delivering energy to nanoscale: Rapid adiabatic transformation, concentration, and stopping of radiation in nano-optics. In eds. N. J. Halas and T. R. Huser, *Plasmonics: Metallic Nanostructures and Their Optical Properties II*, vol. 5512, pp. 38–49. SPIE, Denver, Colorado, (2004).

45. D. K. Gramotnev, Adiabatic nanofocusing of plasmons by sharp metallic grooves: Geometrical optics approach, *J. Appl. Phys.* **98**, 104302–1–11, (2005).

46. S. I. Bozhevolnyi, V. S. Volkov, E. Devaux, J.-Y. Laluet, and T. W. Ebbesen, Channel plasmon subwavelength waveguide components including interferometers and ring resonators, *Nature.* **440**, 508–511, (2006).

47. L. D. Landau and E. M. Lifshitz, *Quantum Mechanics: Non-Relativistic Theory.* (Pergamon Press, Oxford and New York, 1965).

48. L. D. Landau and E. M. Lifshitz, *Electrodynamics of Continuous Media.* (Pergamon,

Mark I. Stockman

Oxford and New York, 1984).

49. C. Cohen-Tannoudji, B. Diu, and F. Laloe, *Quantum Mechanics*. (Wiley, New York, 1977).

50. D. E. Aspnes, S. M. Kelso, R. A. Logan, and R. Bhat, Optical properties of $Al_xGa_{1-x}As$, *J. Appl. Phys.* **60**, 754–767, (1986).

51. P. B. Johnson and R. W. Christy, Optical constants of noble metals, *Phys. Rev. B.* **6**, 4370–4379, (1972).

52. E. N. Economou, Surface plasmons in thin films, *Phys. Rev.* **182**, 539–554, (1969).

53. R. Ruppin, Effect of non-locality on nanofocusing of surface plasmon field intensity in a conical tip, *Phys. Lett. A.* **340**, 299–302, (2005).

54. V. N. Pustovit and T. V. Shahbazyan, Quantum-size effects in sers from noble-metal nanoparticles, *Microelectronics J.* **36**, 559–563, (2005).

55. V. N. Pustovit and T. V. Shahbazyan, Finite-size effects in surface-enhanced raman scattering in noble-metal nanoparticles: A semiclassical approach, *J. Opt. Soc. Am. A.* **23**, 1369–1374, (2006).

56. V. N. Pustovit and T. V. Shahbazyan, Surface-enhanced Raman scattering on the nanoscale: A microscopic approach, *J. Optics A.* **8**, S208–S212, (2006).

57. V. N. Pustovit and T. V. Shahbazyan, SERS from molecules adsorbed on small ag nanoparticles: A microscopic model, *Chem. Phys. Lett.* **420**, 469–473, (2006).

58. V. N. Pustovit and T. V. Shahbazyan, Microscopic theory of surface-enhanced raman scattering in noble-metal nanoparticles, *Phys. Rev. B.* **73**, 085408–1–7, (2006).

59. E. Kretschmann and H. Raether, Radiative decay of nonradiative surface plasmons excited by light, *Z. Naturforsch.* **A 23**, 2135–2136, (1968).

60. H. Raether, *Surface Plasmons on Smooth and Rough Surfaces and on Gratings*. (Springer Verlag, Berlin New York, 1988).

61. J. A. Kong, *Electromagnetic Wave Theory*. (Wiley, New York, 1990).

62. F. Keilmann, Surface-polariton propagation for scanning near-field optical microscopy application, *J. Micros.* **194**, 567–570, (1999).

63. A. Bouhelier, J. Renger, M. R. Beversluis, and L. Novotny, Plasmon-coupled tip-enhanced near-field optical microscopy, *J. Microsc. - Oxford.* **210**, 220–224, (2003).

64. I. A. Larkin, M. I. Stockman, M. Achermann, and V. I. Klimov, Dipolar emitters at nanoscale proximity of metal surfaces: Giant enhancement of relaxation in microscopic theory, *Phys. Rev. B.* **69**, 121403(R)–1–4, (2004).

65. A. Liebsch, Screening properties of a metal surface at low frequencies and finite wave vectors, *Phys. Rev. Lett.* **54**, 67–70, (1985).

66. K. Li, M. I. Stockman, and D. J. Bergman, Self-similar chain of metal nanospheres as an efficient nanolens, *Phys. Rev. Lett.* **91**, 227402–1–4, (2003).

67. E. Verhagen, L. Kuipers, and A. Polman, Enhanced nonlinear optical effects with a tapered plasmonic waveguide, *Nano Lett.* **7**, 334–337, (2007).

68. E. Verhagen, A. Polman, and L. Kuipers, Nanofocusing in laterally tapered plasmonic waveguides, *Opt. Expr.* **16**, 45–57, (2008).

69. C. Ropers, C. C. Neacsu, T. Elsaesser, M. Albrecht, M. B. Raschke, and C. Lienau, Grating-coupling of surface plasmons onto metallic tips: A nano-confined light source, *Nano Lett.* **7**, 2784–2788, (2007).

70. C. Ropers, D. R. Solli, C. P. Schulz, C. Lienau, and T. Elsaesser, Localized multiphoton emission of femtosecond electron pulses from metal nanotips, *Phys. Rev. Lett.* **98**, 043907, (2007).

71. A. Apolonski, P. Dombi, G. G. Paulus, M. Kakehata, R. Holzwarth, T. Udem, C. Lemell, K. Torizuka, J. Burgdoerfer, T. W. Hansch, and F. Krausz, Observation of light-phase-sensitive photoemission from a metal, *Phys. Rev. Lett.* **92**, 073902–1–4,

(2004).

72. D. Zeidler, A. Staudte, A. B. Bardon, D. M. Villeneuve, R. Dorner, and P. B. Corkum, Controlling attosecond double ionization dynamics via molecular alignment, *Phys. Rev. Lett.* **95**, 203003–1–4, (2005).

73. A. Kubo, N. Pontius, and H. Petek, Femtosecond microscopy of surface plasmon polariton wave packet evolution at the silver/vacuum interface, *Nano Lett.* **7**, 470–475, (2007).

74. M. M. Wefers and K. A. Nelson, Programmable phase and amplitude femtosecond pulse shaping, *Opt. Lett.* **18**, 2032–2034, (1993).

75. T. Feurer, J. C. Vaughan, and K. A. Nelson, Spatiotemporal coherent control of lattice vibrational waves, *Science.* **299**, 374–377, (2003).

76. W. Nomura, M. Ohtsu, and T. Yatsui, Nanodot coupler with a surface plasmon polariton condenser for optical far/near-field conversion, *Appl. Phys. Lett.* **86**, 181108–1–3, (2005).

77. L. L. Yin, V. K. Vlasko-Vlasov, J. Pearson, J. M. Hiller, J. Hua, U. Welp, D. E. Brown, and C. W. Kimball, Subwavelength focusing and guiding of surface plasmons, *Nano Lett.* **5**, 1399–1402, (2005).

78. R. J. Mailloux, *Phased Array Antenna Handbook.* (Artech House, Boston, 2005).

79. G. Lerosey, J. de Rosny, A. Tourin, A. Derode, G. Montaldo, and M. Fink, Time reversal of electromagnetic waves, *Phys. Rev. Lett.* **92**, 193904 –1–3, (2004).

80. G. Lerosey, J. de Rosny, A. Tourin, A. Derode, and M. Fink, Time reversal of wideband microwaves, *Appl. Phys. Lett.* **88**, 154101 –1–3, (2006).

81. G. Lerosey, J. de Rosny, A. Tourin, and M. Fink, Focusing beyond the diffraction limit with far-field time reversal, *Science.* **315**, 1120–1122, (2007).
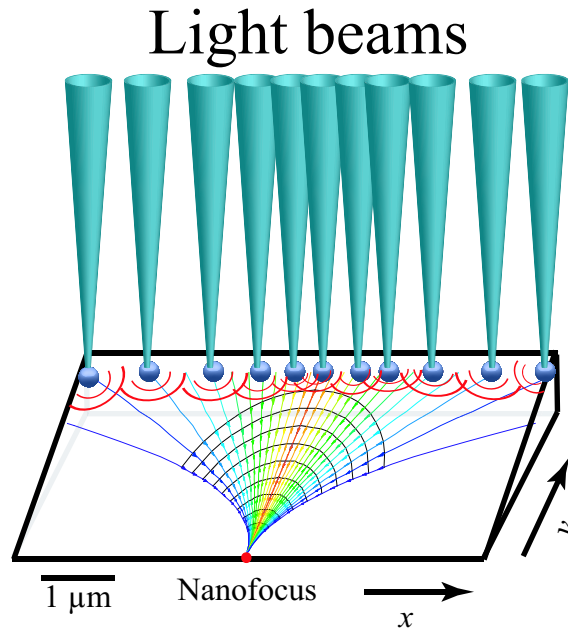
Mark I. Stockman

Light beams

Fig. 16.   Schematic of the full coherent control on the nanoscale or nanoplasmonic active phased array radar (NAPAR). The system consists of plasmonic (silver) nanowedge with nanoparticles (silver nanospheres) positioned at its thick edge. Light beams focused on each of the nanospheres are shown by cones. The omni-directed SPP waves emitted by these excited nanospheres are shown by the red arc segments. The wavefront form by the interference is shown bu concave black curves. Trajectories of SPP rays propagating from the thick to sharp edge of the wedge are shown by color curves, with color coding the initial coordinates. The SPP frequency used in actual computations is $\hbar\omega = 2.5$ eV.
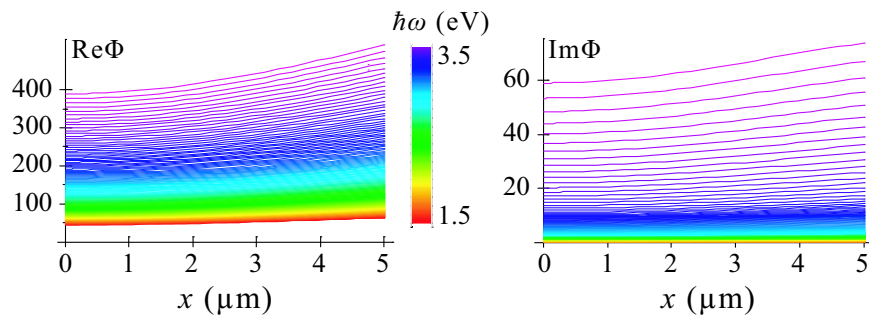

Fig. 17.   (a) Phase (real part of eikonal Φ) acquired by a SPP ray propagating between a point with coordinate x on the thick edge and the nanofocus, displayed as a function of x. The rays differ by frequencies that are color coded by the vertical bar. (b) The same as (a) but for extinction of the ray (Im Φ).
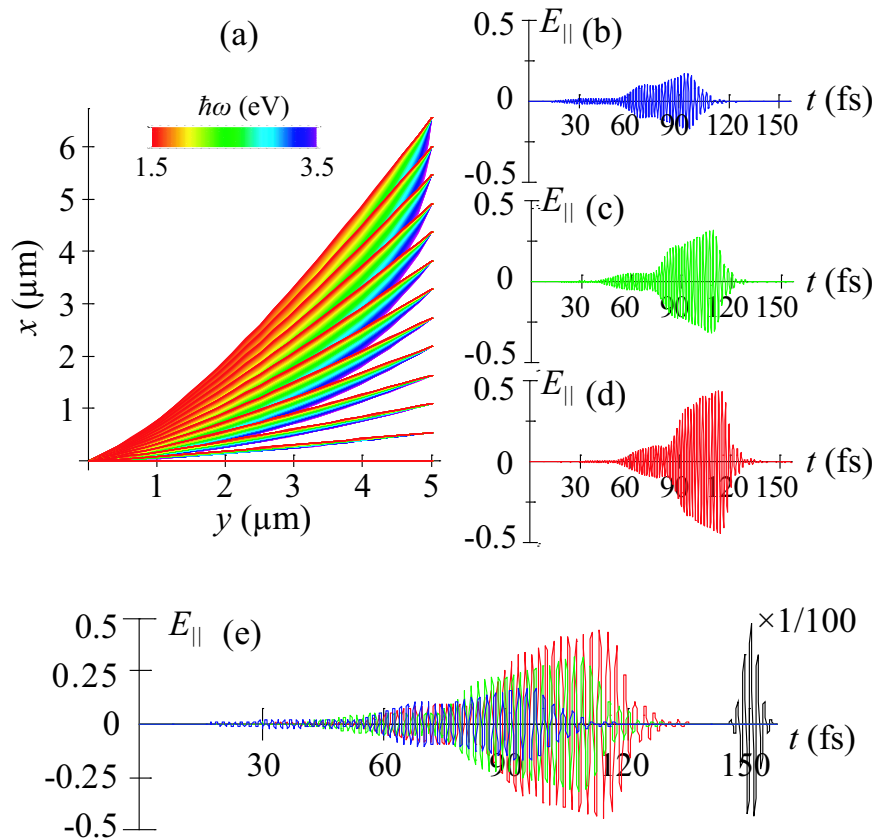
Fig. 18.   (a) Trajectories (rays) of SPP packets propagating from the thick edge to the nanofocus displayed in the xy plane of the wedge. The frequencies of the individual rays in a packet are indicated by color as coded by the bar at the top. (b)-(d) Spatiotemporal modulation of the excitation pulses at the thick edge of the wedge required for nanofocusing. The temporal dependencies (waveforms) of the electric field for the phase-modulated pulses for three points at the thick edge boundary: two extreme points and one at the center, as indicated, aligned with the corresponding x points at panel (a). (e) The three excitation pulses of panels (b)-(d) (as shown by their colors), superimposed to elucidate the phase shifts, delays, and shape changes between these pulses. The resulting ultrashort pulse at the nanofocus is shown by the black line. The scale of the electric fields is arbitrary but consistent throughout the figure.